NASA TECHNICAL NOTE

NASA TN D-6392

NASA TN D-6392

EXPERIMENTAL INVESTIGATION OF A LARGE-SCALE, TWO-DIMENSIONAL, MIXED-COMPRESSION INLET SYSTEM

Performance at Supersonic Conditions, $M_\infty = 1.55$ to 3.2

by Norman D. Wong and Warren E. Anderson

Ames Research Center

Moffett Field, Calif. 94035

NATIONAL AERONAUTICS AND SPACE ADMINISTRATION • WASHINGTON, D. C. • JUNE 1971

1. Report No.	2. Government Accession No.	3. Recipient's Catalog No.
NASA TN D-6392		

4. Title and Subtitle	5. Report Date
EXPERIMENTAL INVESTIGATION OF A LARGE-SCALE, TWO-DIMENSIONAL, MIXED-COMPRESSION INLET SYSTEM Performance at Supersonic Conditions, M_∞ = 1.55 to 3.2	June 1971 6. Performing Organization Code
7. Author(s) Norman D. Wong and Warren E. Anderson	8. Performing Organization Report No. A-3770
9. Performing Organization Name and Address Ames Research Center Moffett Field, Calif. 94035	10. Work Unit No. 720-03-10-03-00-21 11. Contract or Grant No.
12. Sponsoring Agency Name and Address National Aeronautics and Space Administration Washington, D.C., 20546	13. Type of Report and Period Covered Technical Note 14. Sponsoring Agency Code

15. Supplementary Notes

16. Abstract

A large-scale, variable-geometry inlet model with a design Mach number of 3.0 was tested at Mach numbers from 1.55 to 3.2. Variable features of the inlet for off-design operation are an adjustable-height ramp system and a translating cowl. This report presents experimental results for a diffuser and boundary-layer bleed configuration which was optimized at the design Mach number. Overall performance was high with throat-mounted vortex generators, which were effective in reducing flow distortion in the subsonic diffuser at the higher Mach numbers.

17. Key Words (Suggested by Author(s))	18. Distribution Statement
Airbreathing inlets Total-pressure recovery Boundary-layer-bleed systems Vortex generators	Unclassified – Unlimited

19. Security Classif. (of this report)	20. Security Classif. (of this page)	21. No. of Pages	22. Price*
Unclassified	Unclassified	62	$3.00

*For sale by the National Technical Information Service, Springfield, Virginia 22151

SYMBOLS

A	area, in.^{2}
A_c	capture area (196 in.^{2}), defined at $\alpha = 0°$
A_t	throat area, in.^{2}
h	height, in.
h_c	inlet capture height (14 in.)
h_t	throat height, in.
h_{t_u}	unstart throat height, in.
M	Mach number
m	mass flow
m_∞	capture mass flow, $\rho_\infty V_\infty A_c$
m_2/m_∞	main duct (engine) mass-flow ratio
m_{bl}/m_∞	boundary-layer-bleed mass-flow ratio
p	static pressure
p_t	total pressure
$\overline{p}_{t_2}$	area-weighted average total pressure at engine-face station
Δp_{t_2}	distortion index, $\dfrac{p_{t_2\,max} - p_{t_2\,min}}{\overline{p}_{t_2}}$
$\overline{p}_{t_{bl}}$	area-weighted average total pressure at bleed-duct rake station
$\dfrac{\overline{p}_{t_2}}{p_{t_\infty}}$	main-duct total-pressure-recovery ratio
V	velocity, ft/sec
$\dfrac{V_\zeta}{V_0}$	boundary-layer local velocity ratio (referenced to velocity at $h = 1.0$ in.)
α	angle of attack, deg

α_u	angle of attack for inlet unstart, deg
β	angle of yaw, deg
δ_2	deflection angle of ramp number 2, from free stream at $\alpha = 0°$, deg
ρ	mass density, slugs/ft^3

Subscripts

∞	free stream
l	local
1	inlet lip station
2	engine-face station

Vortex Generator Notation

V	vortex generators (height = 5/8 in., $\alpha = 16°$)
RF	ramp location, forward (see fig. 5)

EXPERIMENTAL INVESTIGATION OF A LARGE-SCALE, TWO-DIMENSIONAL, MIXED-COMPRESSION INLET SYSTEM

Performance at Supersonic Conditions, M_∞ = 1.55 to 3.2

Norman D. Wong and Warren E. Anderson

Ames Research Center

SUMMARY

A two-dimensional, mixed-compression, variable-geometry inlet model with a design Mach number of 3.0 was tested at Mach numbers from 1.55 to 3.2. The Reynolds number per foot in this range varied from 4.0×10^6 to 2.0×10^6, respectively.

The effects on inlet performance at the design Mach number of diffuser geometry, porous boundary-layer bleed surfaces, and throat-mounted vortex generators were reported previously. The present report covers the off-design supersonic performance of an inlet configuration selected on the basis of optimum performance at the design Mach number.

Test results cover angles of attack from -2° to +6° and angles of yaw from 0° to 4°. Engine-face total-pressure and bleed-system data indicate that high performance was attained for the complete range of supersonic Mach numbers. Maximum total-pressure recovery at the engine-face station varied from 0.90 at M_∞ = 3.0 to 0.96 at M_∞ = 1.55 for angles of attack and yaw equal to 0°. Diffuser measurements presented include static-pressure distributions, boundary-layer profiles, and wall static-pressure fluctuations.

INTRODUCTION

A general research program has been under way at Ames Research Center to investigate, analytically and experimentally, the overall compression efficiency of a large-scale, two-dimensional inlet system. Studies of supersonic transport missions provided the guidelines for the inlet design criteria. The inlet system is a mixed-compression (external and internal) variable-geometry type with the shock-wave pattern and the overall internal aerodynamic efficiency optimized at the design Mach number of 3.0. The major requirement of high compression efficiency at all Mach numbers up to 3.0 necessitated the use of a boundary-layer bleed system and a variable-height ramp system. A translatable cowl provided efficient external compression and spillage at low off-design Mach numbers. Also, inlet geometry was selected to provide a low-angle external compression surface for minimum spillage drag and a low external cowl angle for reduced cowl pressure drag. The length of the subsonic diffuser was held relatively short to minimize overall propulsion-system weight. Vortex generators were utilized to eliminate diffuser flow separation and reduce flow distortion at the engine-face station.

The inlet system was tested in the Ames Unitary Plan Wind Tunnel at Mach numbers from 0.6 to 3.2. The effects of diffuser geometry, boundary-layer bleed, and vortex generators on inlet performance at the design Mach number, 3.0, are reported in reference 1. Performance of the standard diffuser with an optimum boundary-layer bleed and vortex generator combination is reported here for Mach numbers 1.55 to 3.2. The Reynolds number per foot in this range varied from 4.0×10^6 at $M_\infty = 1.55$ to 2.0×10^6 at $M_\infty = 3.2$.

MODEL, APPARATUS, AND TEST PROCEDURE

A complete description of the two-dimensional inlet research model, apparatus, and test procedure appears in reference 1. Figure 1 shows the model installed in the wind tunnel. Details of the model design are given in figure 2. The inlet was designed so that the theoretical oblique shock wave from the leading edge of the first ramp intersects the leading edge of the cowl lip at a free-stream Mach number of 3.0 for α and $\beta = 0°$. An adjustable ramp assembly and a translatable cowl provide optimum performance at off-design conditions. A fixed conical exit plug with translating sleeve controls the mass flow of the main duct.

Figure 3 shows the relationship of the variable second-ramp angle to the height and area at the minimum throat station. This relationship was identified in reference 1 as normal divergence. Variations in diffuser area ratio are presented in figure 4 for the representative second-ramp angles, δ_2, of 7.0°, 10.0°, and 14.0° for the standard diffuser of reference 1. The local areas are taken in planes normal to the duct centerline. Complete information on the diffuser internal geometry for the design second-ramp angle of 14° is provided in table 1. The equivalent conical angle of the subsonic diffuser at the design condition is about 6.5°.

Boundary layer was removed by a series of replaceable perforated plates mounted on the ramp, sidewall, and cowl internal surfaces. The perforations were equally spaced holes drilled in staggered rows. Boundary-layer-bleed mass flow from the ramp surfaces passed through the plates and into compartmented zones I, II, and III (see fig. 2). In addition, zones II and III served to collect sidewall bleed flow. The compartmented zones were exhausted through circular ducts fitted with remotely controlled exit plugs to provide variable exit areas. The forward sidewall bleed and all cowl bleeds were exhausted directly to the tunnel airstream through manually adjustable exit plates.

The geometry of the boundary-layer bleed system and vortex generators is presented in figure 5. The vortex generators (fig. 5(b)) were designed according to procedures in reference 2. The basic test data presented here are for the 80 VRF configuration in reference 1 (configuration 80 with vortex generators at the forward (throat) position on the ramp). The plate perforations for this configuration are identified in table 2, where porosity is defined as the ratio of total hole area to total plate area in percent.

Test instrumentation included flush static-pressure orifices along the centerline of the ramp and cowl internal surfaces, and along the mid-duct line of the internal sidewalls. Boundary-layer rakes were located at three stations on the ramp and at two stations on both the cowl and right-hand sidewall (fig. 5(a)). Pressure cells (transducers) for measuring static-pressure fluctuations were mounted on the mid-duct line at four sidewall stations including the engine face (fig. 5(b)).

Boundary-layer-bleed mass flow and total-pressure recovery were determined from rake measurements of static and total pressure near the exit of each bleed duct. Total-pressure measurements from the engine-face rakes were area weighted to determine main-duct total-pressure recovery. Recovery values were then used to calculate mass-flow ratio by the choked-plug method in which uniform choked flow conditions were assumed at the exit plug minimum-area station.

RESULTS AND DISCUSSION

Inlet Compression Efficiency

Engine-face performance– The basic compression efficiency performance of the two-dimensional inlet research model using configuration 80 VRF optimized at $M_\infty = 3.0$ is plotted in figure 6. Total-pressure-recovery ratio and distortion index are plotted against total boundary-layer-bleed mass-flow ratio for free-stream Mach numbers from 3.2 to 1.55. Angle of attack and angle of yaw were fixed at 0°, and the throat heights for maximum pressure recovery were selected at each Mach number by the procedure described in reference 1. Bleed mass-flow ratio increased as the exit area of the main duct was closed down to move the terminal shock wave forward toward the throat. Maximum bleed mass-flow ratios are reached just prior to inlet unstart, which is characterized by a sudden movement of the terminal shock wave upstream to an external position. The unstart condition is discussed at the end of this section under flow unsteadiness. Figure 6(a) cover tests at Mach numbers of 2.5 and above. It shows a trend of decreasing maximum recovery and increasing boundary-layer-bleed mass-flow ratio as Mach number is increased up to and including the overspeed Mach number 3.1. The maximum total-pressure recovery at the design Mach number, 3.0, was 0.90 for a bleed mass-flow ratio of 0.146. Further overspeed to $M_\infty = 3.2$ severely reduces the maximum total-pressure recovery attainable because it was not possible mechanically to adjust the ramps to a physical throat height consistent with the higher contraction ratio required for high pressure recovery at that Mach number. The data in figure 6(a) (dashed curves) show that the stable range of subcritical mass-flow ratios was extended beyond the maximum recovery point at $M_\infty = 2.75$ and 2.50, the reason being that the combination of small area variation in the throat region and throat bleed allows the terminal shock wave to position upstream of the geometric throat, thus increasing shock-wave losses. Distortion characteristics at normal inlet operating conditions are generally low ($\Delta p_{t_2} < 0.10$) and are independent of Mach number between 2.50 and 3.10.

Below $M_\infty = 2.50$ (fig. 6(b)), maximum total-pressure recovery is further increased with decreasing Mach number down to $M_\infty = 2.0$. Distortion performance deteriorates rather rapidly, however, and the index value for maximum recovery at $M_\infty = 2.0$ is almost double the value at $M_\infty = 2.5$. The cause is a viscous effect that will be discussed in the next paragraph. For $M_\infty = 2.0$ and below the throat height was held constant. At $M_\infty = 1.75$ and 1.55 it was necessary to retract the cowl from its design position to avoid excessive internal contraction. Only a partial retraction of the cowl (to model station 46.44) was necessary at $M_\infty = 1.75$ to maintain internal supersonic compression up to $m_{bl}/m_\infty = 0.066$. The unstart discontinuity is indicated by the dashed recovery curve. Fully retracting the cowl allowed the inlet to operate at $M_\infty = 1.55$ as a normal external-compression system with negligible internal contraction. A maximum recovery ratio of about 0.96 was then attained with a bleed mass-flow ratio as low as about 0.09.

Figure 7 shows the total-pressure-ratio contours, at the engine-face station, for maximum total-pressure recovery at each of the indicated Mach numbers. The contours indicate the basic nature of two-dimensional inlet systems of this type in which the area along the diffuser length is varied by curving the ramp. The flow in the high-energy core is not mixed uniformly across the duct between the cowl and ramp surfaces. Since the flow at the engine face station is shown to be essentially symmetrical about the duct vertical centerline, flow asymmetry about the horizontal axis is shown most clearly by total-pressure-ratio profiles measured by the vertical centerline rake at the engine-face station. Figure 8 shows profiles for four of the Mach numbers considered in figure 7. The profiles are identified with figure 6 data by the values of total-pressure recovery. Included in figure 8 is the profile corresponding to maximum recovery conditions with the vortex generators removed (configuration 80). For this case, an examination of the data suggests possible separated flow on the ramp surface at $M_\infty = 3.0$ and 2.5, since the wall static pressure was approximately equal to or greater than the local total pressure.[1] The addition of vortex generators eliminated separation at both Mach numbers and increased recovery at $M_\infty = 3.0$. At $M_\infty = 2.0$ and 1.55, the data show that no flow separation exists; therefore vortex generators are unnecessary. It is at these Mach numbers, however, that viscous effects have a predominant effect on the distortion index. At $M_\infty = 2.0$ the engine-face Mach number is high relative to that at $M_\infty = 3.0$ because of increased mass flow; consequently, the duct static pressure is lower relative to the total pressure. Total pressure measurements within the boundary layer approach the wall static pressure value and reflect the flow conditions (distortion index, fig. 6(b)) as being greatly distorted when, in fact, the flow outside the boundary layer is relatively free of distortion (see fig. 8(c)). Retracting the cowl at Mach numbers less than 2.0 relieves this effect since increased spillage decreases the engine-face mass flow and Mach number, thus increasing the static pressure at the wall.

The inlet compression efficiency parameters at maximum total-pressure recovery are summarized in figure 9 in which results are compared for the standard bleed configuration (80) with and without vortex generators. Also included is a reduced bleed configuration (24) (ref. 1) which has a short subsonic diffuser and no vortex generators. Total pressure recovery for this configuration is less than for the standard bleed configuration (80); distortion is slightly higher in the range above $M_\infty = 2.5$ and lower in the range below. Vortex generators could be expected to improve both of these performance parameters on the basis of their favorable effect on the longer diffuser with standard bleed. For example, at $M_\infty = 3.0$ the addition of vortex generators increased the maximum recovery from 0.885 to 0.90 and reduced the associated distortion index from 0.115 to 0.08. Below $M_\infty = 2.50$, vortex generators did not improve pressure recovery but did continue to reduce distortion.

The "adjusted" curve in figure 9 shows how the distortion index is affected when the total-pressure measurements within the boundary layer are excluded. The distortion index for the "adjusted" curve was calculated by arbitrarily eliminating the total-pressure probe measurements made within 0.50 inch of the duct surfaces. These results indicate that the core flow distortion is insensitive to free-stream Mach number.

Inlet flow angularity – The effects of inlet flow angularity (angle of attack and angle of yaw) on the inlet compression efficiency parameters are shown in figure 10 for representative Mach numbers. These effects at maximum total-pressure recovery conditions are summarized in figure 11. The model boundary-layer-bleed system was not altered during angle excursions, but the throat

[1] Refer to reference 1, figure 14, for larger scale plot of data at $M_\infty = 3.0$.

height was optimized for best recovery at each test angle condition. After the inlet was started, the main duct exit area was held fixed at a sufficiently large value that it would not contribute to an inlet unstart. The throat height was then decreased until unstart occurred. This throat height was noted and defined as the unstart throat height. Two throat height ratios are listed in figure 10 for each combination of α and β. The first (h_t/h_{t_u}) is the ratio of the maximum recovery throat height to the unstart throat height. The second ($h_{t_u}/h_{t_{u_{\alpha=0}}}$) is the ratio of the unstart throat height (for the indicated α and β) to the unstart throat height at α and $\beta = 0°$. The increase in unstart throat height with increasing angle of attack is consistent with the increase in duct mass-flow ratio indicated by the m_2/m_∞ curves of figure 10. Both effects result from the increase in effective capture areas as the inlet is pitched to positive angles of attack. The duct mass-flow ratio curves (m_2/m_∞) are used with engine airflow requirements to determine inlet sizing and inlet-engine matching performance.

Maximum recovery performance at α and β for a range of Mach numbers is shown in figure 11. Generally, increasing angle of attack decreases maximum total-pressure recovery and increases boundary-layer-bleed mass-flow ratio. Angle of yaw is shown to be more detrimental to recovery than angle of attack at the higher Mach numbers; however, bleed mass-flow ratio is relatively unaffected, and the distortion index is not substantially affected by either flow angle variation. Optimum inlet-engine matching along the curves shown in figure 11 would require a variable ramp control system that is sensitive to both free-stream Mach number and inlet-flow angularity. Also, a bypass system would be required in the subsonic diffuser. Understandably, in a practical situation an inlet operating with an engine would operate at lower than maximum recovery and at a correspondingly lower bleed mass flow to provide a control tolerance.

At angles of attack of 4° and 6°, operating the inlet system at $M_\infty = 2.0$ resulted in serious performance degradation (see fig. 10(c)). The lower limit of operation with the cowl fully extended is $M_\infty = 2.0$, and for this condition wedge-flow theory predicts reflected shock-wave detachment on the ramp (number 2) surface at an angle of attack of about 6°. Complete inlet unstart was not observed although the data indicate this to be the case. It is possible, however, that increased boundary-layer-bleed mass-flow ratio associated with $\alpha = 4°$ and 6° could have compensated for internal shock-wave detachment to prevent or reduce the severity of the unstart condition. Some cowl retraction could be beneficial in delaying the unstart to a higher angle of attack.

The throat height ratio, h_t/h_c, for maximum recovery and for inlet unstart is shown in figure 12 for several angles of attack over a Mach number range from 2.0 to 3.0. As indicated previously, the throat height ratio for either condition increases with increasing angle of attack and decreasing Mach number. For $\alpha = 0°$ the throat height for maximum recovery at $M_\infty = 2.0$ is about twice the height at the design Mach number, 3.0. Similar increases are required for the other angles of attack.

An important requirement for an inlet is resistance to throat unstart which can be caused by angle-of-attack transients similar to those associated with a passing aircraft or gusts. If sufficient tolerance to sudden flow fluctuations is not provided, angle-of-attack transients will cause the inlet to unstart because of the limited reaction time of inlet control and actuation systems. To indicate the tolerance of the inlet system to angle of attack, cross plots of the unstart curves at three free-stream Mach numbers are shown by the inset curves shown in figure 12. Superimposed on the

inset curves is a curve drawn through the throat height values for maximum recovery for $\alpha = 0°$ at each Mach number. The angles of attack corresponding to these values represent the attainable angles before throat unstart occurs when throat heights are set for maximum recovery at $\alpha = 0°$. The angles for throat unstarts are 0.8°, 1.4°, and 2.25° at $M_\infty = 3.0$, 2.75, and 2.5, respectively. No determination of this tolerance was attempted for $M_\infty = 2.0$ since the unstart indications were unreliable at $\alpha = 4°$ and 6°. Operating the inlet below maximum recovery by increasing the operating throat height would provide a corresponding increase in unstart angle-of-attack tolerance as indicated by the slope of the inset curves. The results are qualitative since the dynamic characteristics of the transients and the dynamic response of the inlet system were not simulated.

Diffuser Measurements

Boundary-layer bleed system– Representative inlet mass-flow ratios are shown in figure 13 for maximum total-pressure recovery conditions at $\alpha = 0°$ and 4° for Mach numbers from 1.55 to 3.0. As shown, the total inlet mass-flow ratio is the sum of the engine and bleed mass-flow ratios. Also shown are curves for calculated total inlet mass-flow ratios. The calculations accounted for cowl spillage only; no estimation was made of spillage over the sidewall leading edges. It is evident from the figure that the calculated and experimental values compare reasonably well. The lack of agreement at $\alpha = 4°$ occurs in the low range of Mach numbers where sidewall spillage would be greatest.

Data pertaining to boundary-layer-bleed distribution are shown in figure 14. Ramp bleed (R) in bleed zone I and sidewall plus ramp bleed (SW + R) in bleed zones II and III were measured by means of pressure instrumentation in the respective bleed ducts. Calibration factors derived from these measurements were applied in calculating the bleed quantities[2] that were not measured directly. In general, in bleed zones I and II, bleed mass-flow ratios remained essentially constant through a range of Mach numbers from 2.0 to 3.2. Bleed levels for $M_\infty = 1.55$ and 1.75 were less than at the higher Mach numbers because of the reduced compression with cowl retraction. In bleed zone III, the cowl bleed (C) remained essentially constant throughout the Mach number range, while the sidewall plus ramp bleed (SW + R) increased linearly with increasing Mach number. This trend is carried over to the uppermost curve in figure 14, which represents the total bleed throughout the test Mach number range. As mentioned previously, a Mach number of 2.0 represents the lower limit of operation with the cowl fully extended, and internal shock-wave detachment could be responsible for the higher total bleed at this Mach number. At the lower Mach numbers (1.55 and 1.75) for which the cowl was retracted, some change in the total bleed mass-flow ratio would be expected because of changing shock-wave patterns and reduced cowl bleed area.

The variation of bleed-duct total-pressure ratio with Mach number is shown in figure 15. The trend of the curve for bleed duct 2 is quite similar to the smooth curve for bleed duct 1, except for the effect of cowl retraction at $M_\infty = 1.75$ and 1.55. In contrast to these curves, the variation of pressure ratio with Mach number for bleed duct 3 indicates some irregularities at $M_\infty = 2.5$ and below. These can be attributed to the special bleed duct required for testing in this range of Mach numbers. A constriction introduced into the internal surface of the duct for the purpose of sting clearance distorted the flow at the rake measuring station and reduced recovery.

[2] These quantities were for forward sidewall (zone I) and cowl bleeds in zones II and III. Cowl bleed in zone I was blanked off.

Static-pressure distributions– The distribution of static-pressure ratio along the ramp, sidewall, and cowl for maximum recovery is shown in figure 16 for several free-stream Mach numbers. For $M_\infty = 2.5$ and above the data show that the terminal shock-wave pressure rise was localized near the design throat station (58.8). The major pressure rise at $M_\infty = 2.0$ is forward of the throat (fig. 16(c)) which gives credulity to the earlier suggestion that the oblique shock wave is detached in the supersonic diffuser at this Mach number. Operating the inlet at $M_\infty = 1.55$ provides a single pressure rise, which is caused by an external terminal shock wave forward of the fully retracted cowl lip (model station 52.0). Subsonic diffusion is minimal at Mach numbers of 2.0 and below because the diffuser area change with model station is small (see $\delta_2 = 7°$, fig. 4).

Boundary-layer characteristics– Boundary-layer profiles of total-pressure ratio, Mach number, and velocity ratio are presented in figures 17, 18, and 19, respectively. The local total-pressure ratio profiles at three duct stations are shown in figure 17. Data for the configuration without vortex generators (designated 80) are included at the downstream location only, since data at the other stations are not affected by the vortex generators. Similarly, the upstream profiles are insensitive to terminal shock wave (recovery) effects. At the design Mach number (3.0), the upstream rake measurements show a boundary-layer thickness of about 0.25 inch on both the ramp and cowl surfaces. By comparison, the sidewall thickness is about twice this value. A similar trend in relative boundary-layer thickness and profile exists at the throat rake location. Local total-pressure ratios measured within the throat inviscid core flow were within about 0.02 of the throat theoretical shock-recovery value of 0.95 on all three surfaces. Downstream profiles indicate relatively uniform, attached flow on the ramp surface when vortex generators were used. For the condition of maximum engine-face recovery (0.90), the maximum local total-pressure ratio measured by the downstream rake was about 0.86. The mixing process within the subsonic diffuser increased this value to 0.875 at the engine face (at about an inch from the ramp surface) as indicated in figure 8(a).

Reducing the free-stream Mach number to 2.5 and 2.0 generally provided local boundary-layer characteristics similar to those at $M_\infty = 3.0$. One difference is the reduced sidewall boundary-layer thickness at the upstream rake station. Also, the downstream profile without vortex generators at $M_\infty = 2.0$ shows significant improvement over that measured at $M_\infty = 3.0$ and 2.5. Further reducing free-stream Mach number to 1.55 produces characteristics peculiar to the external compression process that was used when the cowl was retracted. As the terminal shock wave moves forward on the ramp, the subsonic Mach number at the upstream rake station decreases and the flow exhibits an increasing tendency toward separation. Engine-face total-pressure recovery increases with the forward movement of the shock wave because the boundary-layer bleed system is effective in reestablishing attached, high-recovery flow at the throat station. For the most forward position (indicated by $\bar{p}_{t_2}/p_{t_\infty} = 0.936$) of the terminal shock wave in figure 17(d) the throat profile indicated low energy distorted flow which is manifested in the sharp drop in engine-face recovery shown in figure 10(d).

Throat total-pressure profiles have been converted to local Mach number profiles in figure 18 to better assess the flow conditions at the entrance to the subsonic diffuser. A discussion of low supersonic throat Mach numbers at supercritical flow conditions was included in reference 1. The point was made that difficulty in measuring static pressure accurately in the throat probably accounted for the local Mach number being less than 1.1 when predictions indicate the value should approach 1.2. Figure 18 indicates the above characteristic is present at all supersonic Mach

numbers. Low subsonic throat Mach numbers shown were measured as a result of high boundary-layer bleed rates in the region between the throat rake and the terminal shock wave.[3]

The effectiveness of vortex generators in preventing flow separation at the downstream ramp location is illustrated more clearly by the boundary-layer velocity profiles in figure 19. The forced-mixing effect of vortex generators is dramatically displayed at all Mach numbers particularly at $M_\infty = 3.0$ and 2.5. Strongly attached boundary layers are clearly evident when the vortex generators are added. On the other hand, the shape of the profiles obtained without vortex generators at these Mach numbers indicates incipient flow separation.

Flow unsteadiness– Diffuser static-pressure unsteadiness is shown in figure 20 at four stations (three transducer stations are indicated in fig. 5). Oscillograph traces are shown for both maximum recovery and unstart conditions at $M_\infty = 3.0$, 2.5, and 2.0, and for maximum recovery and minimum subcritical conditions at $M_\infty = 155$. At each of the high Mach numbers, the inlet was brought to a stable operating condition for maximum recovery and then unstarted by decreasing the main mass-flow control area. Pressure cell 4 was located at the engine face station and showed negligible unsteadiness at maximum recovery for all Mach numbers. At $M_\infty = 3.0$ and 2.5, maximum pressure amplitude at the throat region (pressure cell 2) was about 8 and 5 percent of the free-stream total pressure, respectively. For unstart conditions, maximum amplitudes for both throat and engine-face station were approximately 18 percent at $M_\infty = 3.0$ and 22 percent at $M_\infty = 2.5$. At $M_\infty = 2.0$ the throat region pressure amplitude for maximum recovery increased to about 0.11 p_{t_∞}, while for the unstart condition the throat amplitude reached 0.34 p_{t_∞}. However, the engine-face station amplitude at the unstart condition was only about 0.03 p_{t_∞}. This result also contributes to the difficulty in understanding the internal flow at this Mach number. However, the unsteadiness characteristics shown can be explained by large terminal shock-wave excursions in the throat region usually associated with a partially unstarted inlet. At $M_\infty = 1.55$ the throat region pressure amplitude was about 0.16 p_{t_∞} at maximum recovery. The minimum subcritical operating condition suffers from excessive unsteadiness at all pressure cell locations which ranged from 0.30 p_{t_∞} at the forward location to 0.18 p_{t_∞} at the engine face. Low-energy flow in the subsonic diffuser was indicated earlier by throat profile measurements and could explain the excessive levels of unsteadiness that were experienced.

CONCLUDING REMARKS

The results of an experimental investigation of a two-dimensional mixed-compression inlet system with a design Mach number of 3.0 have been presented for a range of supersonic Mach numbers from 1.55 to 3.2. A variable ramp system and a translating cowl provided for off-design operation. Boundary-layer bleed was provided by a series of perforated plates on the internal surfaces of the ramps, sidewalls, and cowl. Data presented are primarily for a selected configuration (80 VRF) consisting of a standard length subsonic diffuser used in combination with vortex generators mounted in the throat region and a boundary-layer bleed system optimized at the design Mach number. For angles of attack and yaw equal to 0° the measured maximum total-pressure recovery at the engine-face station varied from 0.90 at $M_\infty = 3.0$ to about 0.96 at $M_\infty = 1.55$. The

[3] Low throat Mach numbers at $M_\infty = 1.55$ were due to external spillage.

boundary-layer-bleed mass-flow ratios associated with these values of recovery were 0.146 and 0.080, respectively. Values of distortion index adjusted for viscous effects were well below 0.10 for the full range of test Mach numbers. At $M_\infty = 3.0$, the supersonic portion of the inlet performed nearly as predicted inasmuch as the total-pressure recovery indicated at the throat rake station was within 0.02 of the theoretical value of 0.95. Flow distortion and possible separation existed in the subsonic diffuser at $M_\infty = 3.0$ and 2.5. Vortex generators just downstream of the throat were effective in producing a strong forced-mixing action that decreased distortion considerably at the engine-face station.

In general, as angle of attack was increased, the maximum total-pressure recovery decreased while the total boundary-layer-bleed mass-flow ratio increased. At the design Mach number, a pressure recovery loss of 0.02 was indicated when the angle of attack was increased to 4°. Angle of yaw was found to be more harmful to recovery than angle of attack at high Mach numbers. Neither of the inlet flow angularities (α or β) substantially affected the distortion index.

The resistance of the inlet to throat unstart due to angle-of-attack transients was determined. For the design Mach number of 3.0 when the throat height was set for maximum recovery at zero angle of attack, the inlet unstart angle of attack was 0.8°. This value increased to 2.25° at $M_\infty = 2.50$. Static-pressure unsteadiness was determined to be negligible at the engine-face station during operation at maximum recovery conditions throughout the supersonic Mach number range. During the unstart conditions, however, the unsteadiness was the order of 20 percent of the free-stream total pressure.

Ames Research Center
National Aeronautics and Space Administration
Moffett Field, California, 94035, March 10, 1971

REFERENCES

1. Anderson, Warren E.; and Wong, Norman D.: Experimental Investigation of a Large-Scale, Two-Dimensional, Mixed-Compression Inlet System – Performance at Design Conditions, $M_\infty = 3.0$. NASA TM X–2016, 1970.

2. Taylor, Harlan D.: Summary Report on Vortex Generators. United Aircraft Corp. Department Report R–05280–9, March 7, 1950.

TABLE 1.– DESIGN COORDINATES, $\delta_2 = 14°$

[All dimensions are in inches]

Model station	Height station		Duct height	Duct width	Fillet radius	
	Ramp surface	Cowl surface			Ramp surface	Cowl surface
0	0			14.00		
	*					
28.00	3.438					
30.40	*	14.00				
54.14	9.954					
55.00	10.158					
56.00	10.367					
57.00	10.533					
58.00	10.615					
58.80	10.645		3.355			
60.28			3.355			
61.76			3.368			
63.24			3.394			
64.72			3.432			
65.52	10.544		3.456			
66.50			3.482			
67.85			3.535			
69.52			3.632			
71.12			3.763			
72.00	10.147		3.853			
73.74		*	3.92			
74.50		13.80	*			0
77.62			4.31			.29
80.00	9.19		4.61			.56
81.52			4.82		0	.76
82.50			4.97		.15	.91
85.00	8.40		5.40		.58	1.29
87.50			5.89		1.09	1.80
90.00	7.36		6.44		1.62	2.39
92.50			7.04		2.22	2.92
95.52	5.94		7.86		3.04	3.50
97.50			8.40		3.58	3.84
99.33			8.86		4.03	4.11
101.36	4.52	13.86	9.34		4.48	4.38
102.50		13.91	9.59		4.69	4.53
105.00	3.92	14.08	10.16	*	5.08	4.91
107.28		14.38	10.76		5.38	5.38
110.00	3.26	*	11.48		5.74	5.74
113.02			12.28	12.80	6.14	6.14
115.02	2.60	15.40	12.80	12.80	6.40	6.40

*Straight line between points

TABLE 2.– BOUNDARY-LAYER-BLEED PLATE SCHEDULE (CONFIGURATION 80 VRF)

		Plate number						
		1	2	2X	3	4	5	6
Ramp	Hole diam. in.	0.125	0.078	N.A.[b]	0.125	0.078	Blank	Blank
	Porosity, percent	13	7.6[a]		19.6	7.6		
Sidewall	Hole diam. in.	0.125	0.125	N.A.	0.125	0.125	Blank	Blank
	Porosity, percent	13	13		19.6	13		
Cowl	Hole diam. in.	Blank	0.125	0.125	0.078	N.A.	N.A	N.A.
	Porosity, percent		13[c]	13[c]	7.6[d]			

[a]Aft 4 in., holes filled.

[b]Not applicable.

[c]Every other two rows of holes filled.

[d]Aft half, holes filled.

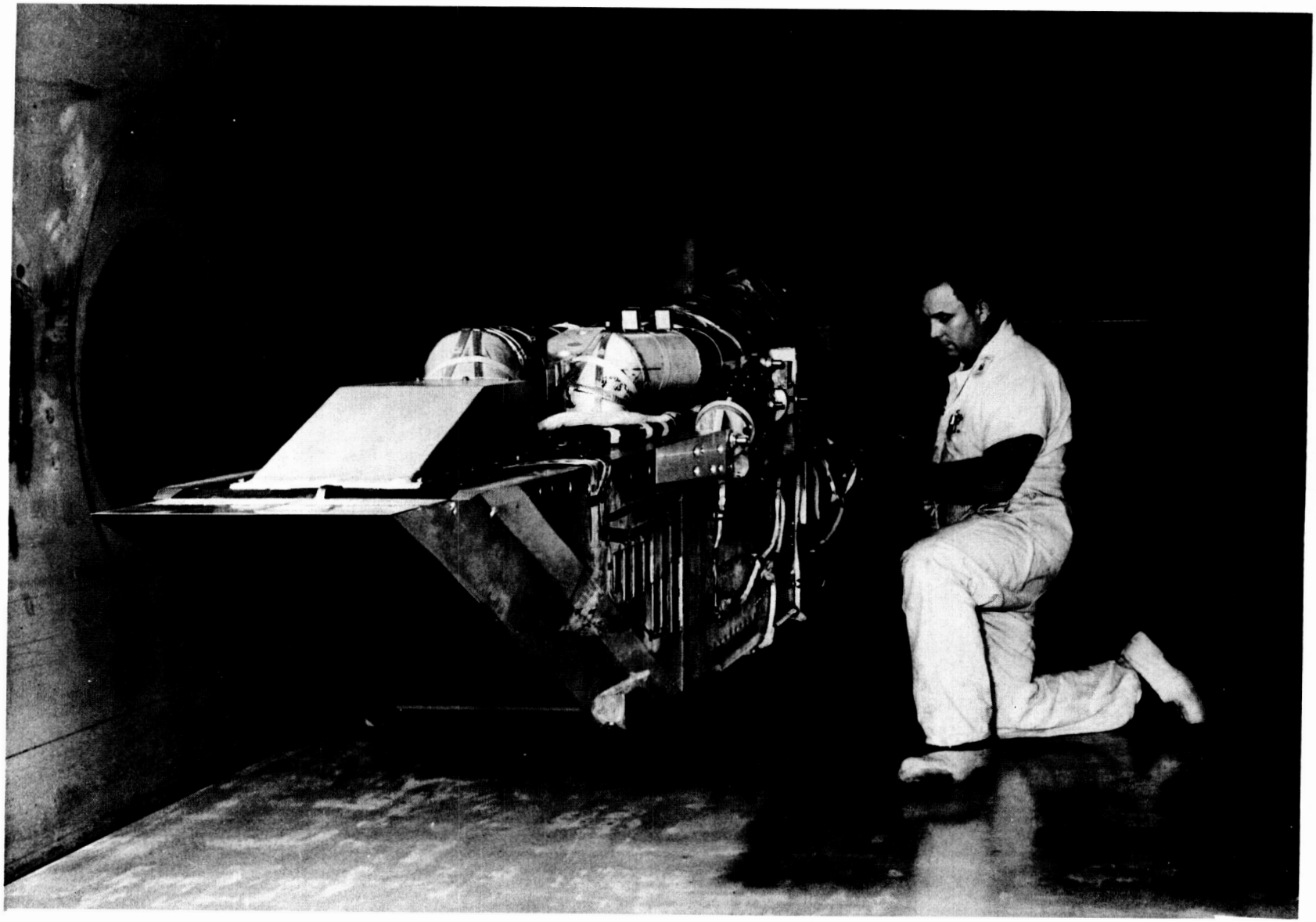

A-32238

Figure 1.- The two-dimensional inlet research model installed in the Ames Unitary Plan Wind Tunnel.

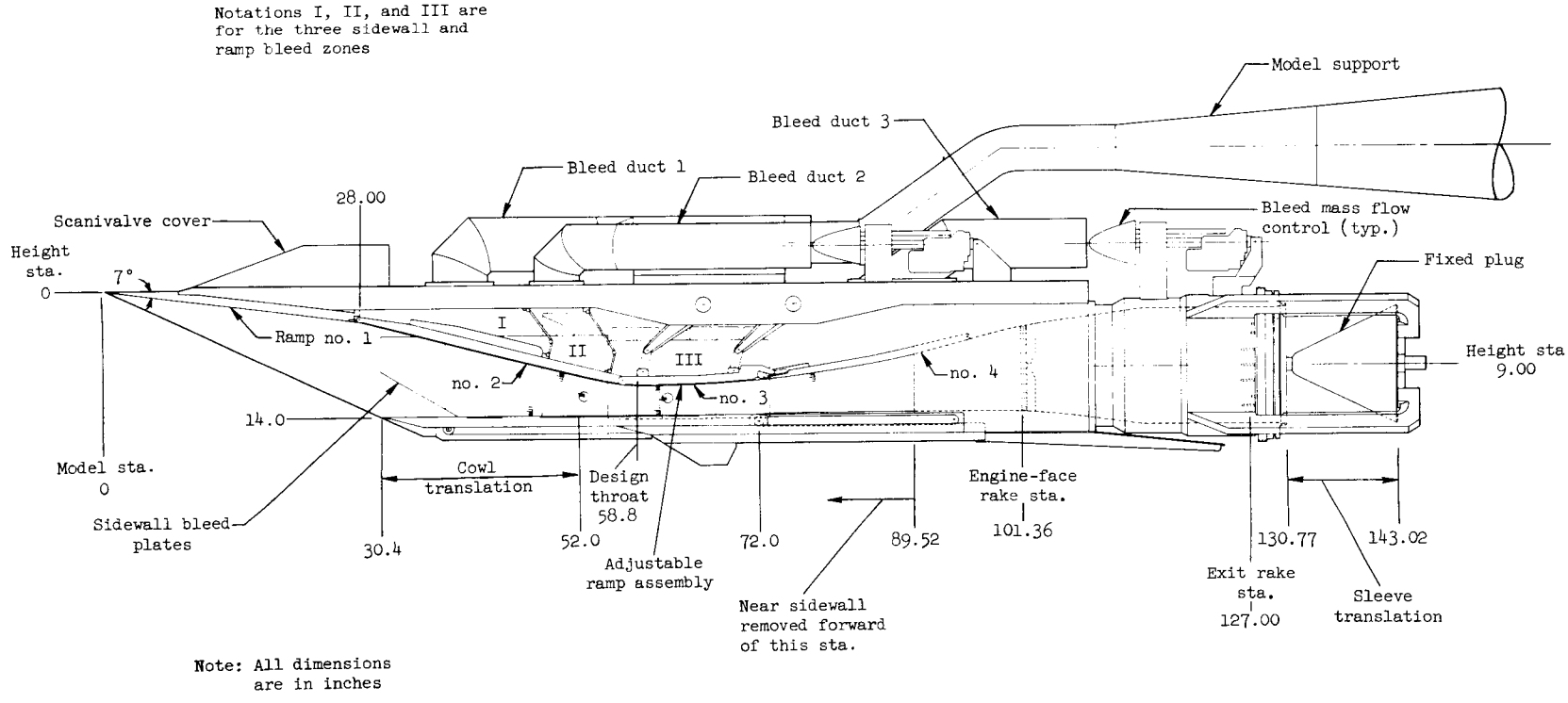

Figure 2.- A drawing of the two-dimensional inlet research model.

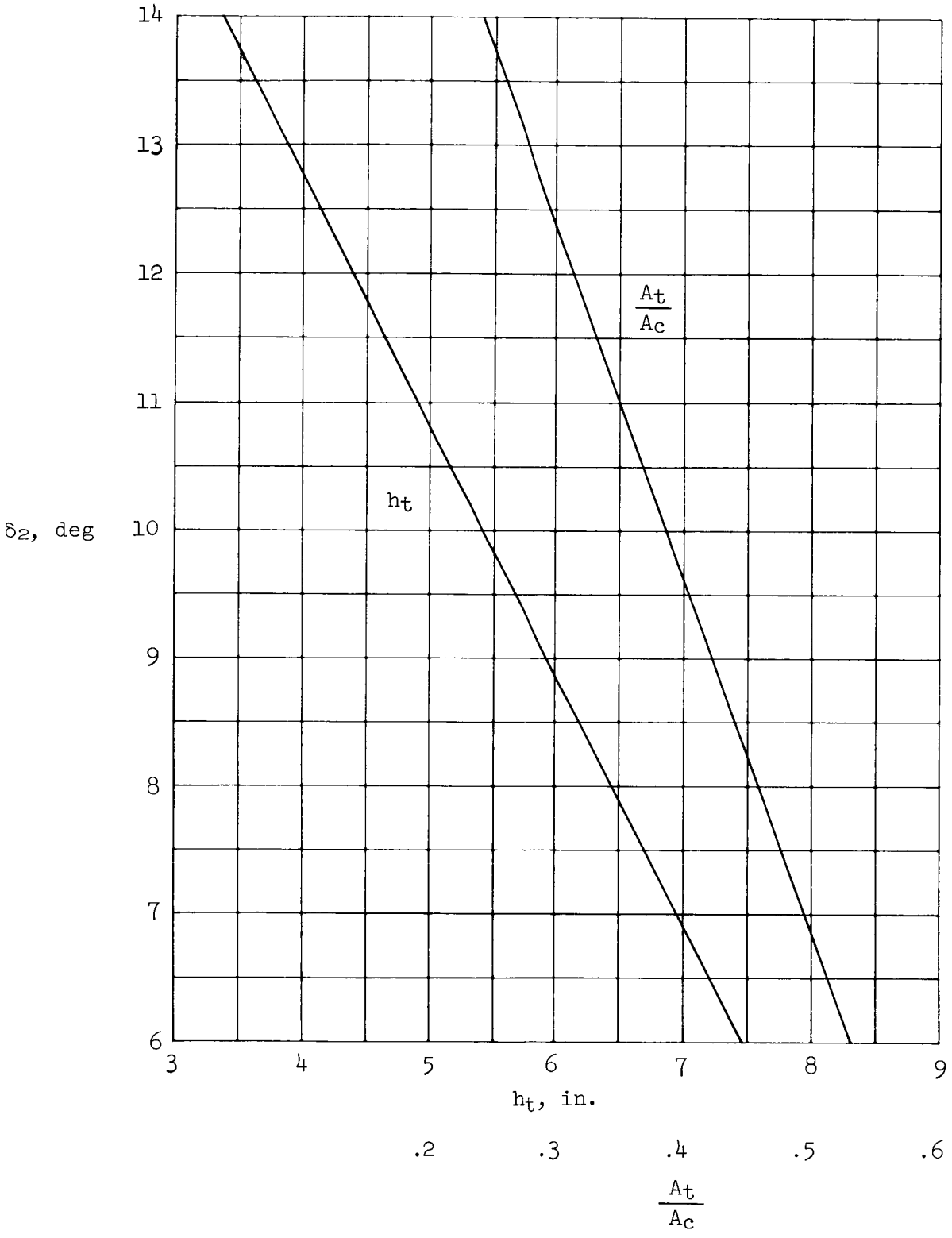

Figure 3.- Relationship of second-ramp angle to height and area ratio at the throat station (normal divergence).

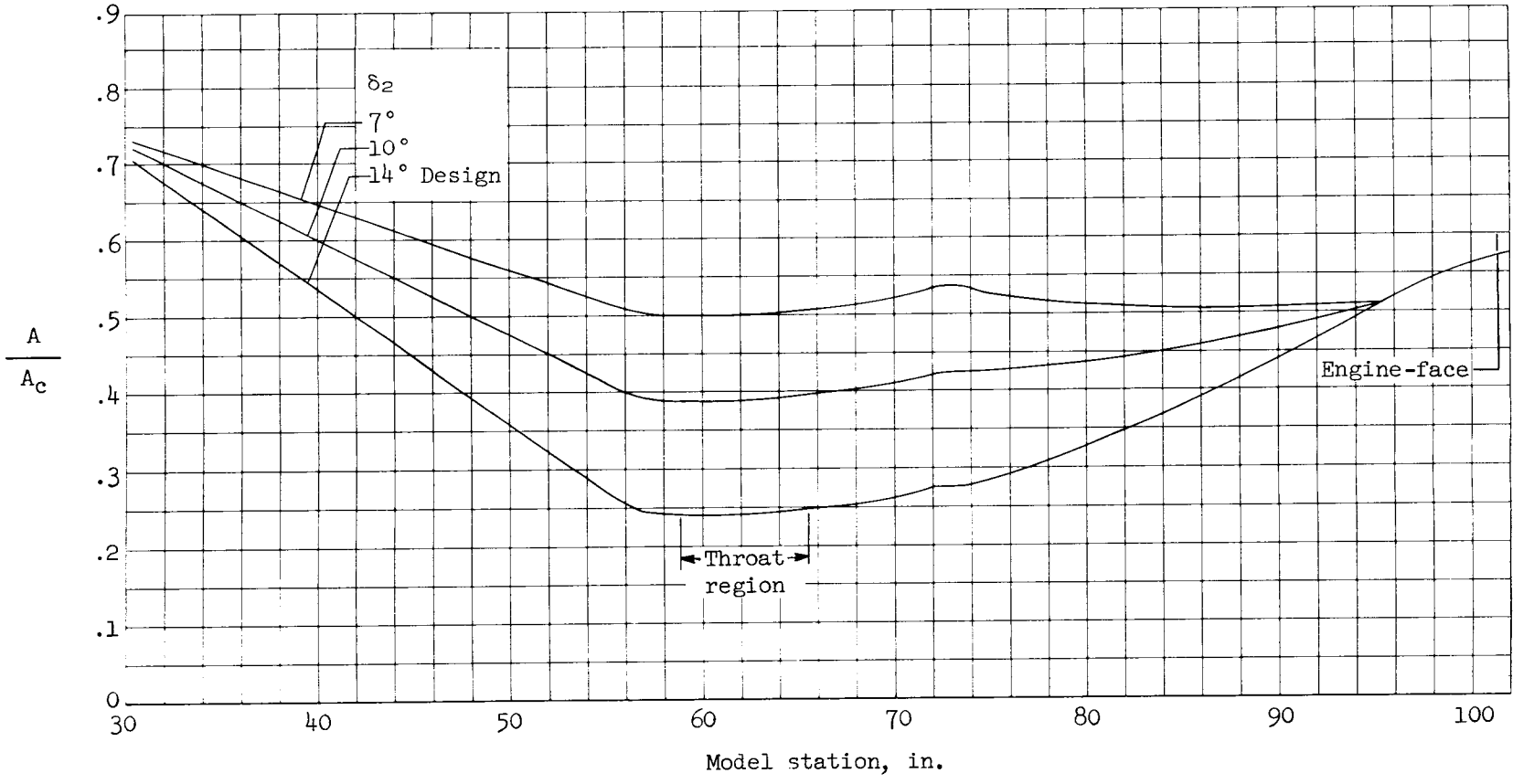

Figure 4.- Diffuser area-ratio variation (standard diffuser).

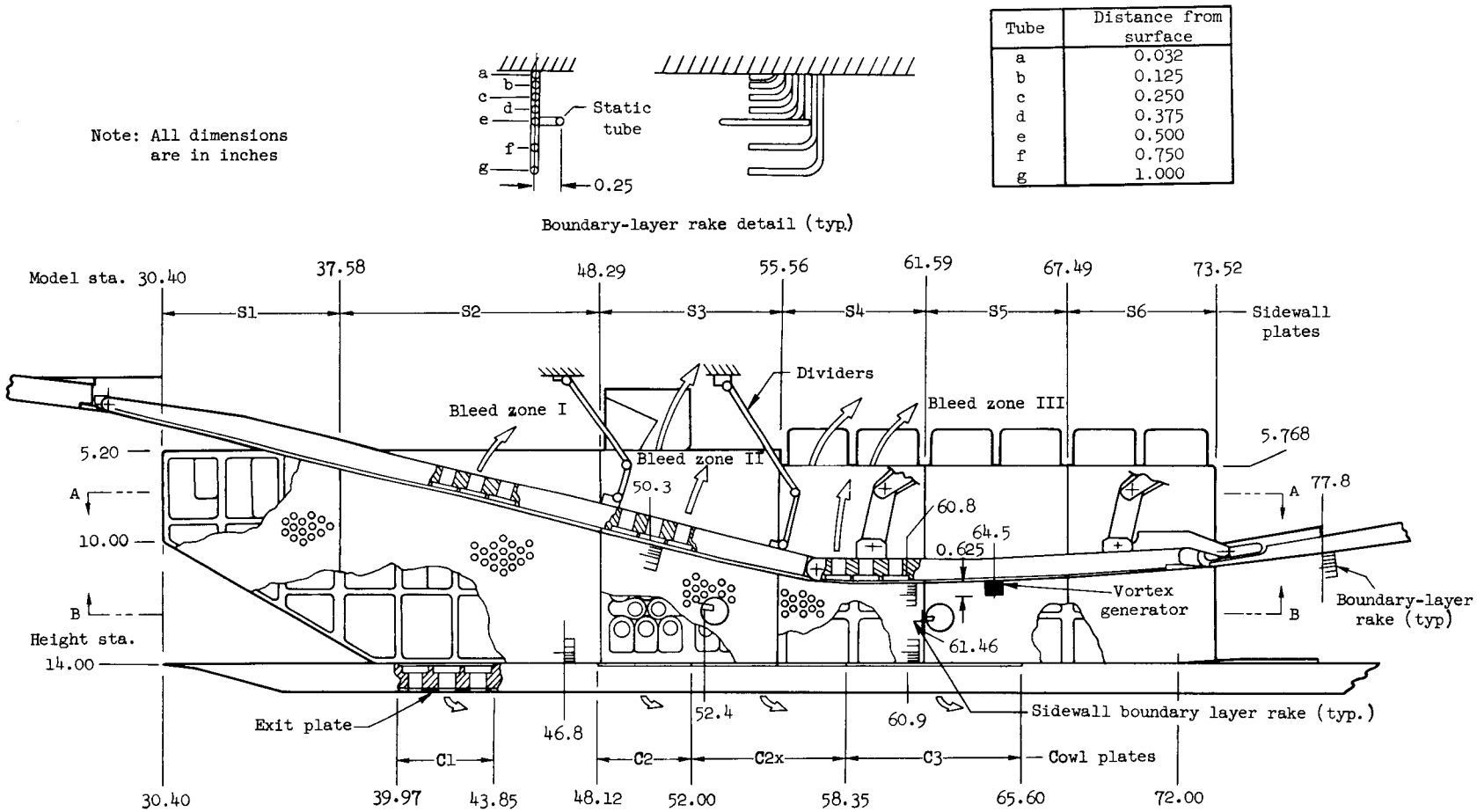

(a) Side view

Figure 5.- Details of the boundary-layer bleed system; design throat height.

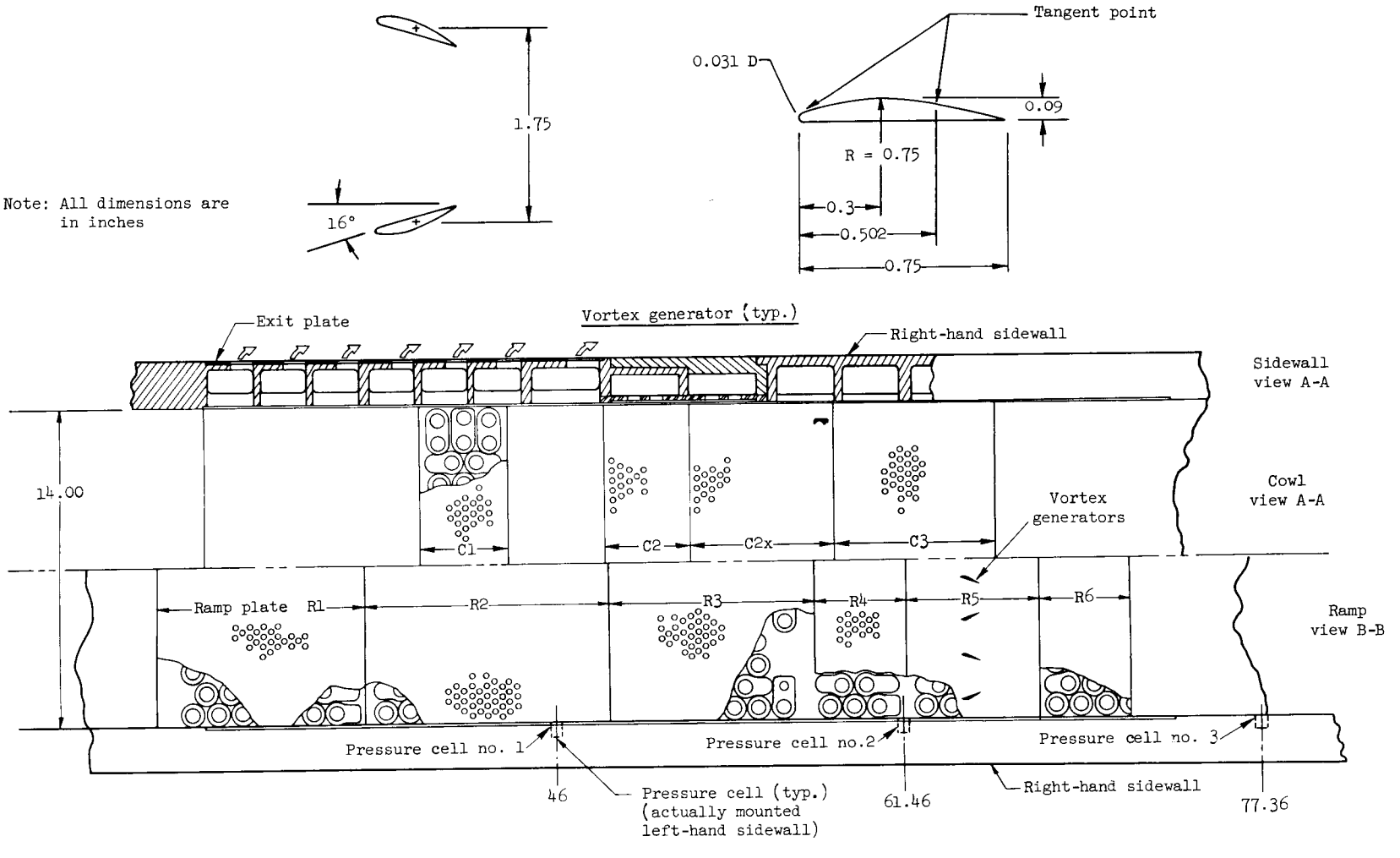

(b) Plan view

Figure 5.- Concluded.

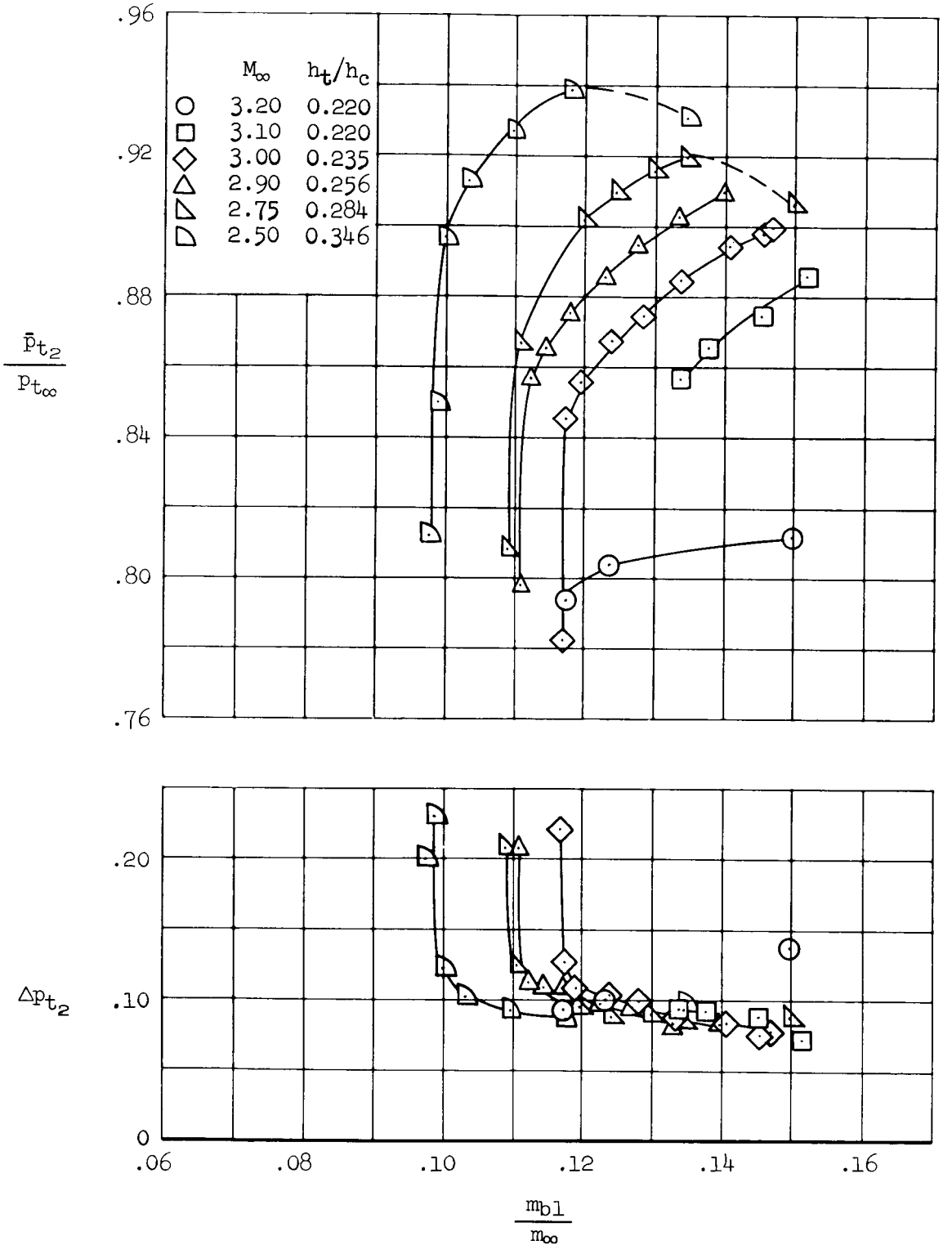

(a) M_∞ = 2.50-3.20

Figure 6.- Inlet compression-efficiency performance; α = 0°, β = 0°.

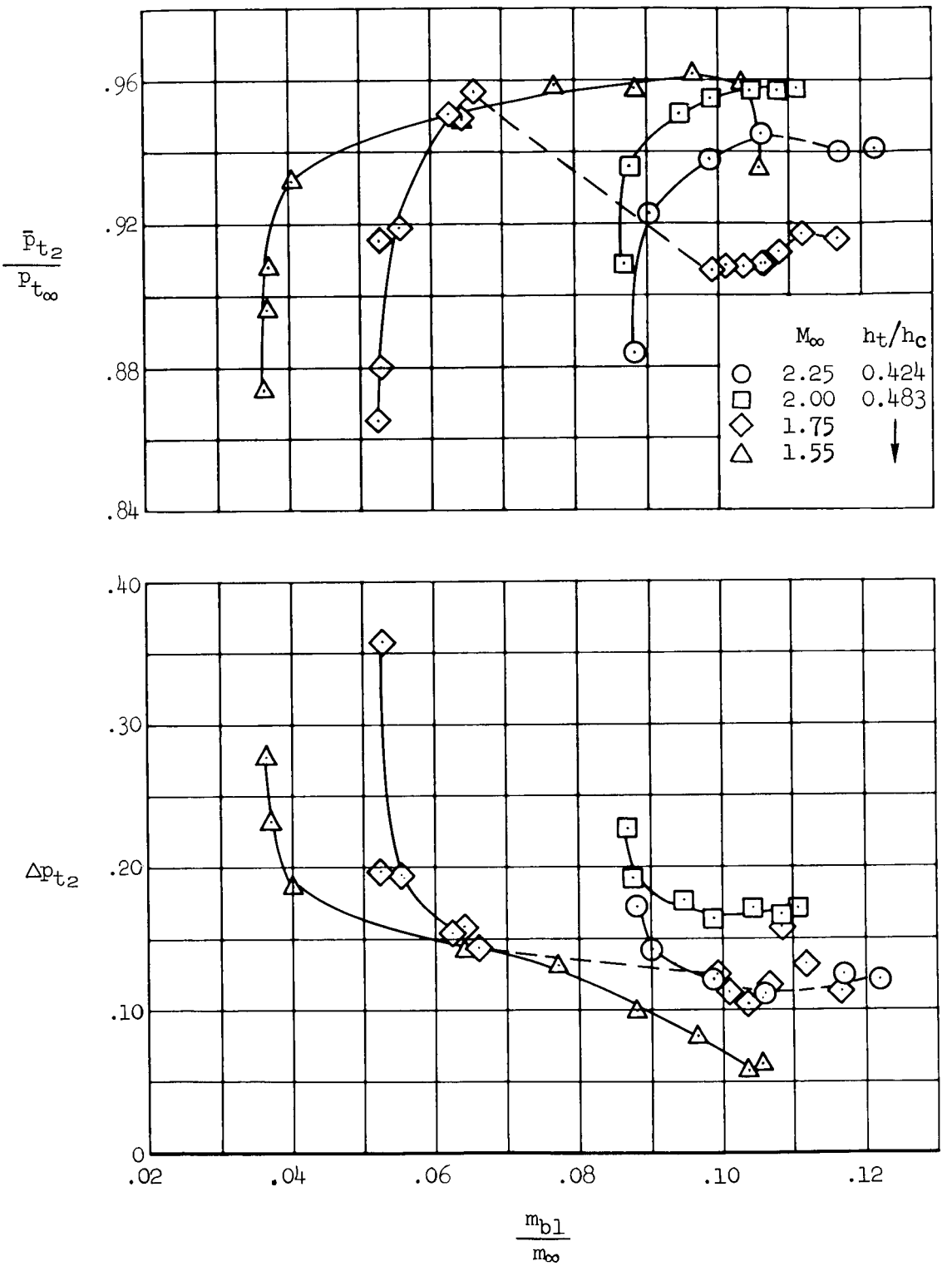

(b) M_∞ = 1.55-2.25

Figure 6.- Concluded.

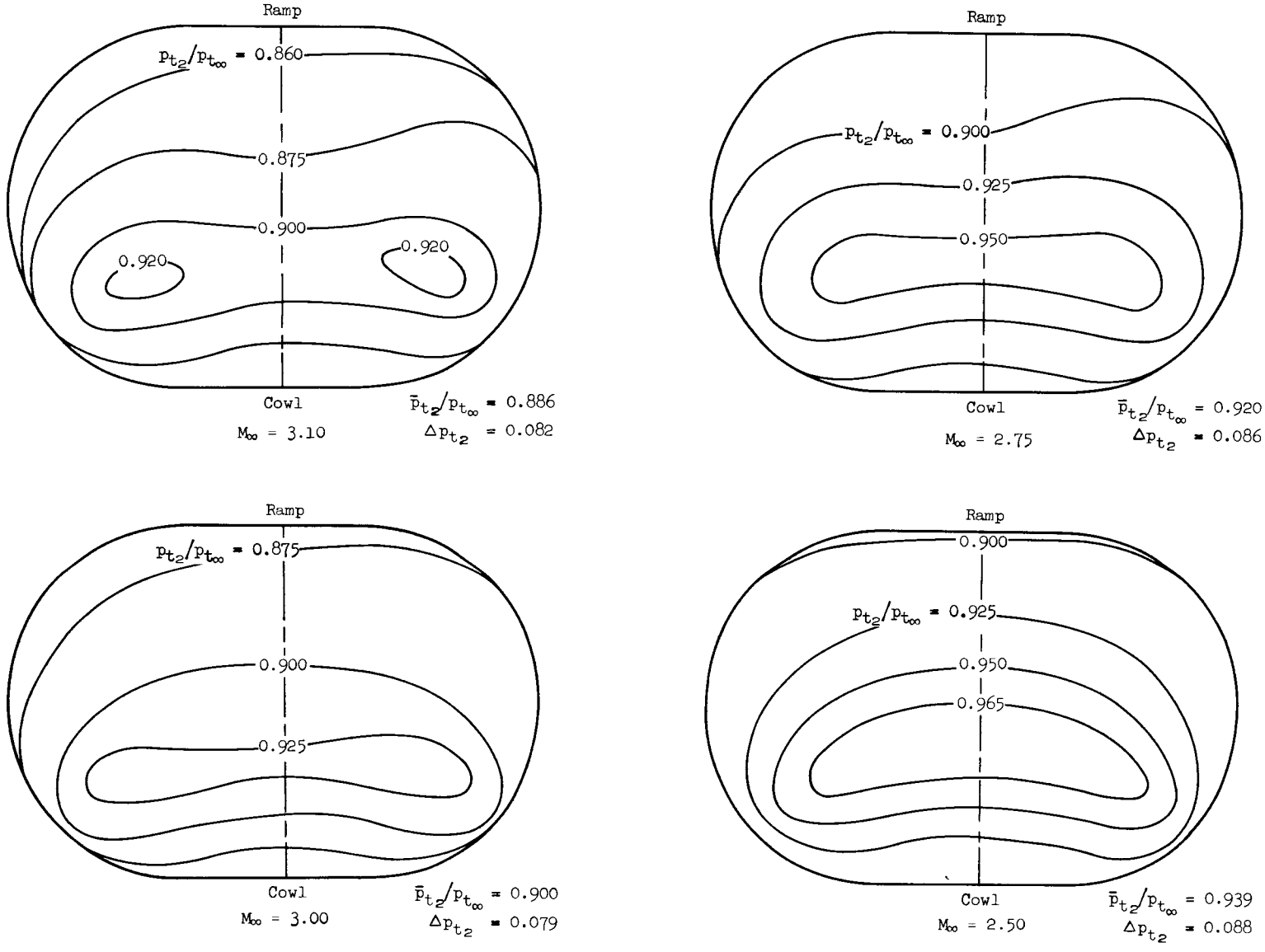

(a) M_∞ = 2.50-3.10

Figure 7.- Engine-face total-pressure contours for maximum total-pressure recovery; α = 0°, β = 0°.

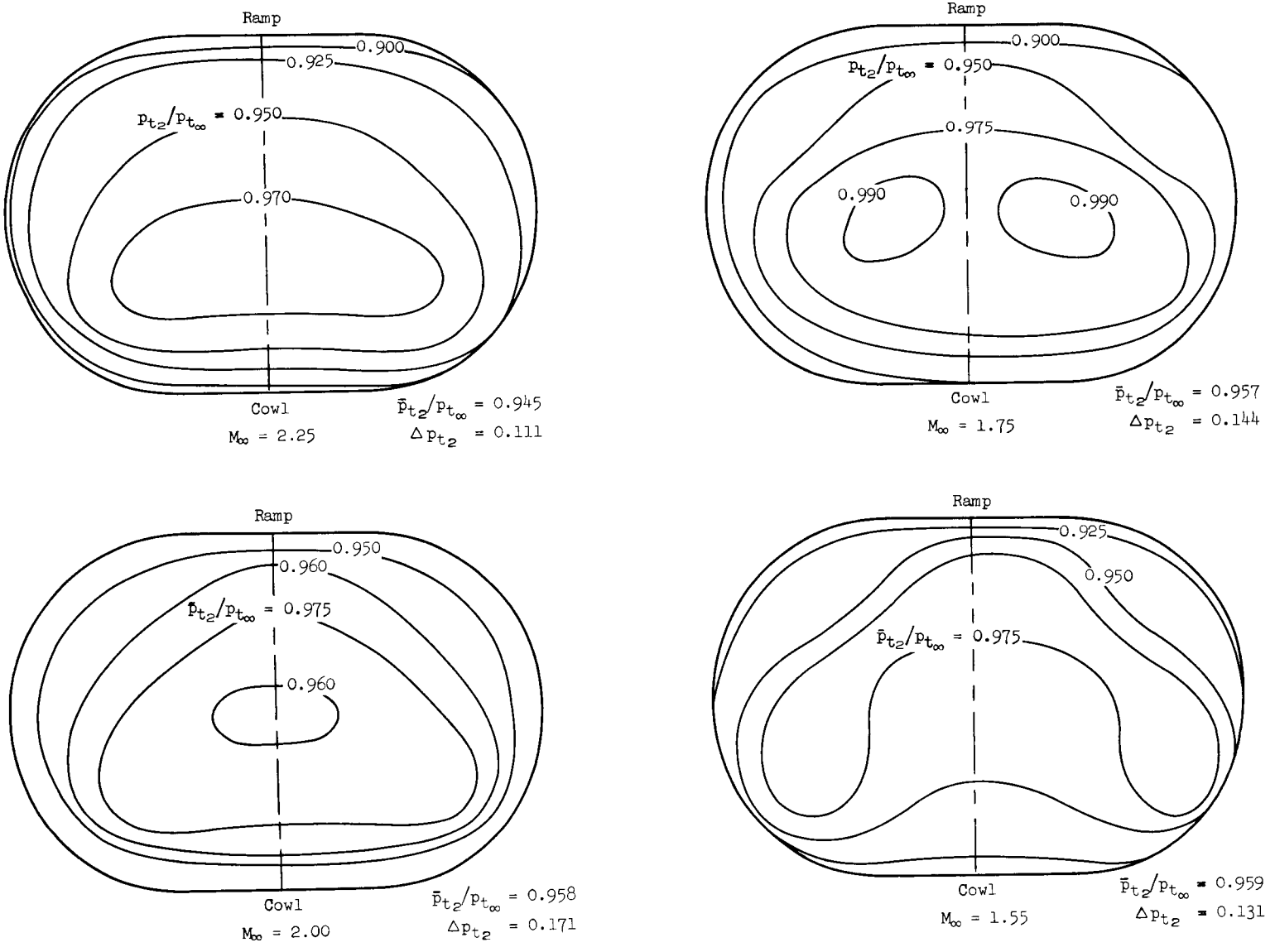

(b) M_∞ = 1.55-2.25

Figure 7.- Concluded.

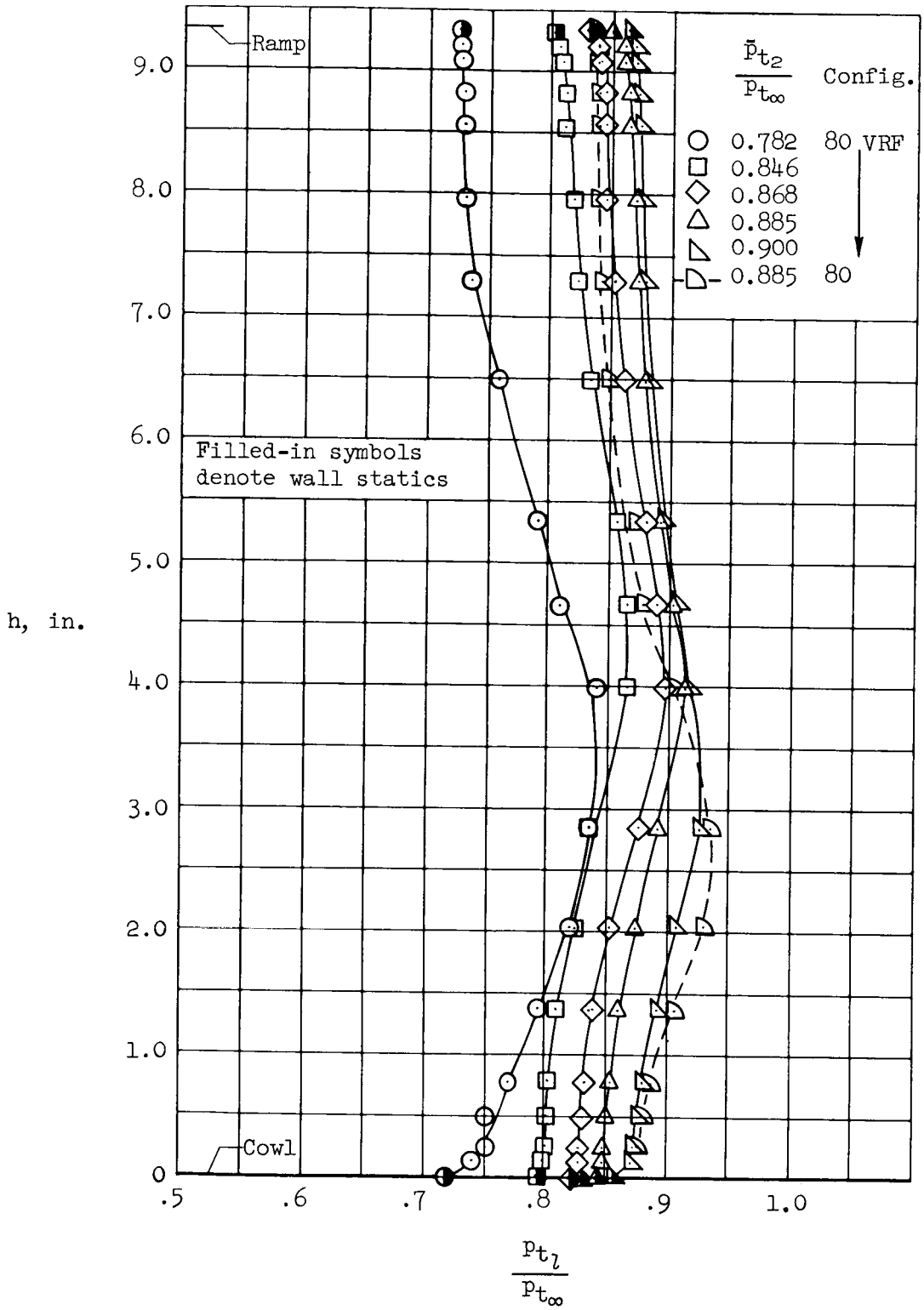

(a) $M_\infty = 3.00$

Figure 8.- Vertical engine-face total-pressure profiles; $\alpha = 0°$, $\beta = 0°$.

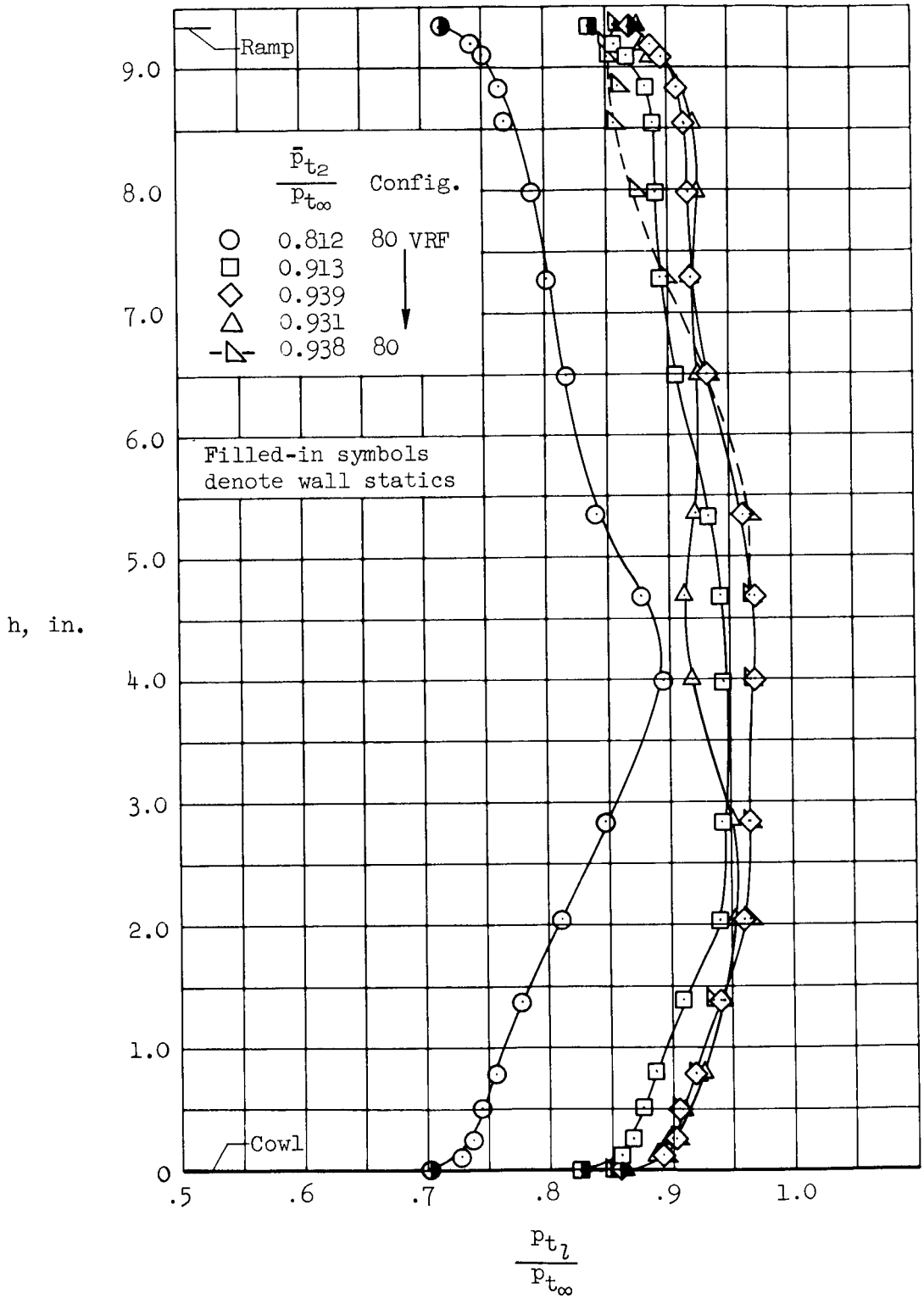

(b) $M_\infty = 2.50$

Figure 8.- Continued.

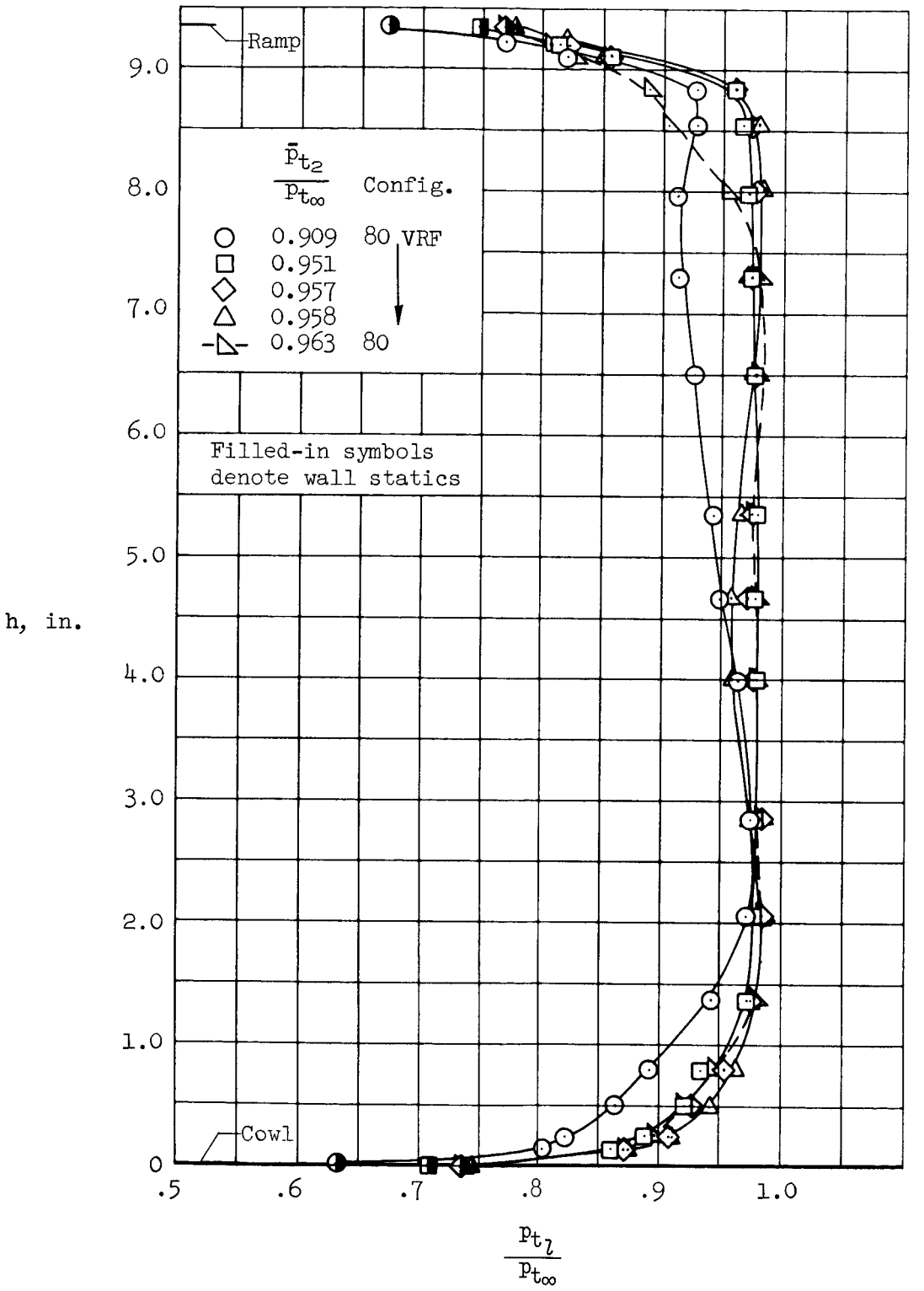

(c) $M_\infty = 2.00$

Figure 8.- Continued.

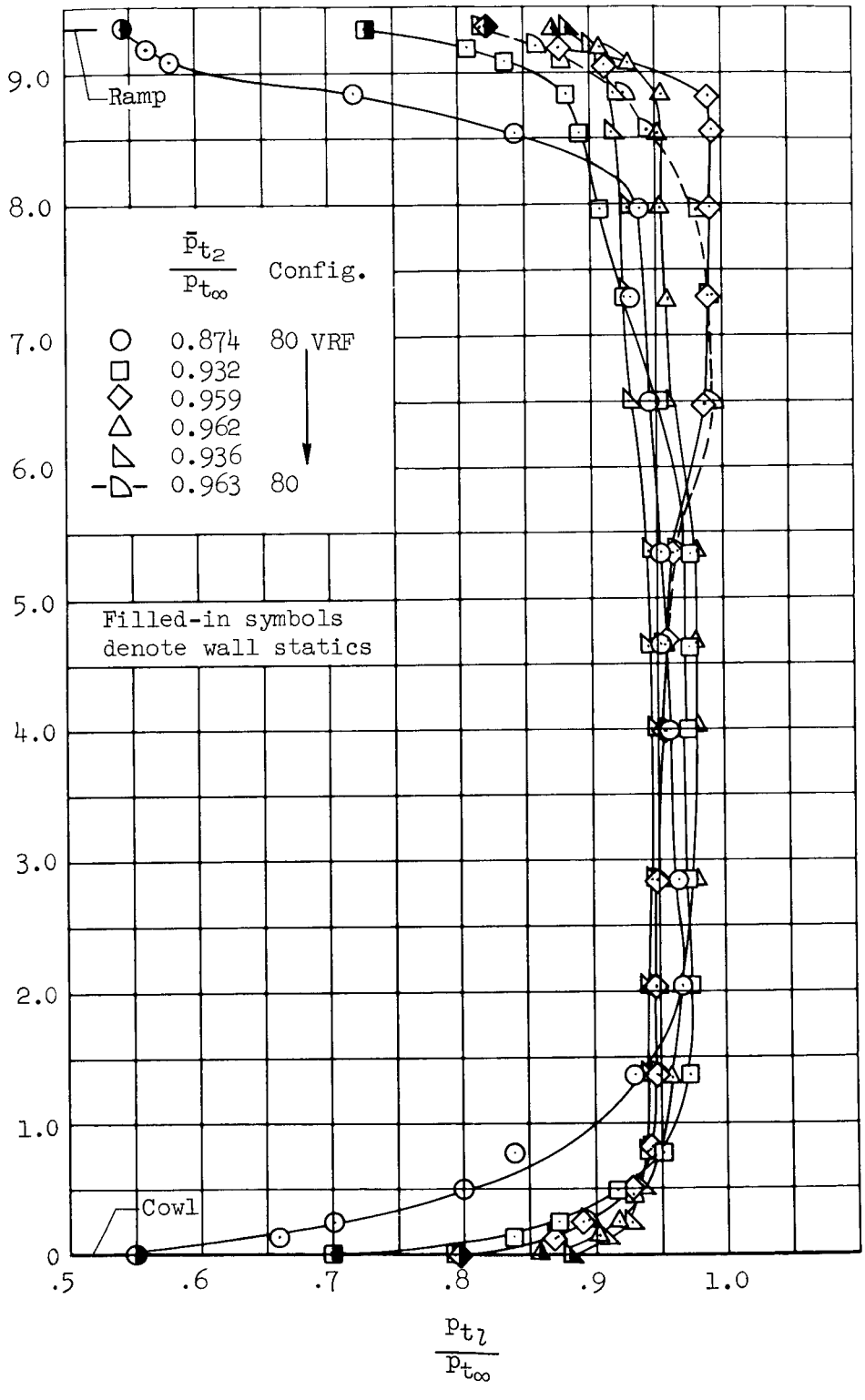

(d) $M_\infty = 1.55$

Figure 8.- Concluded.

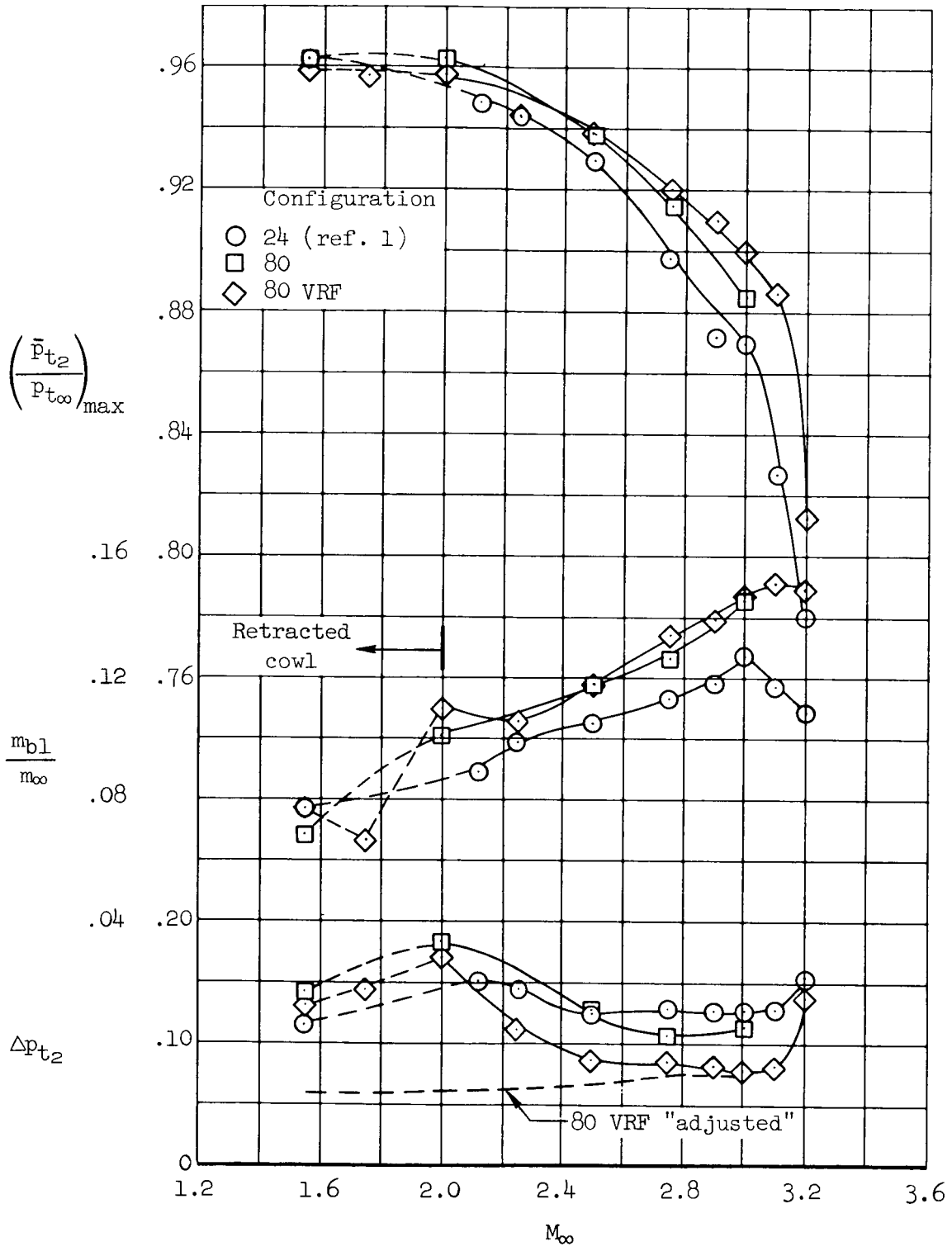

Figure 9.- The effect of Mach number on inlet compression-efficiency parameters for maximum total-pressure recovery; $\alpha = 0°$, $\beta = 0°$.

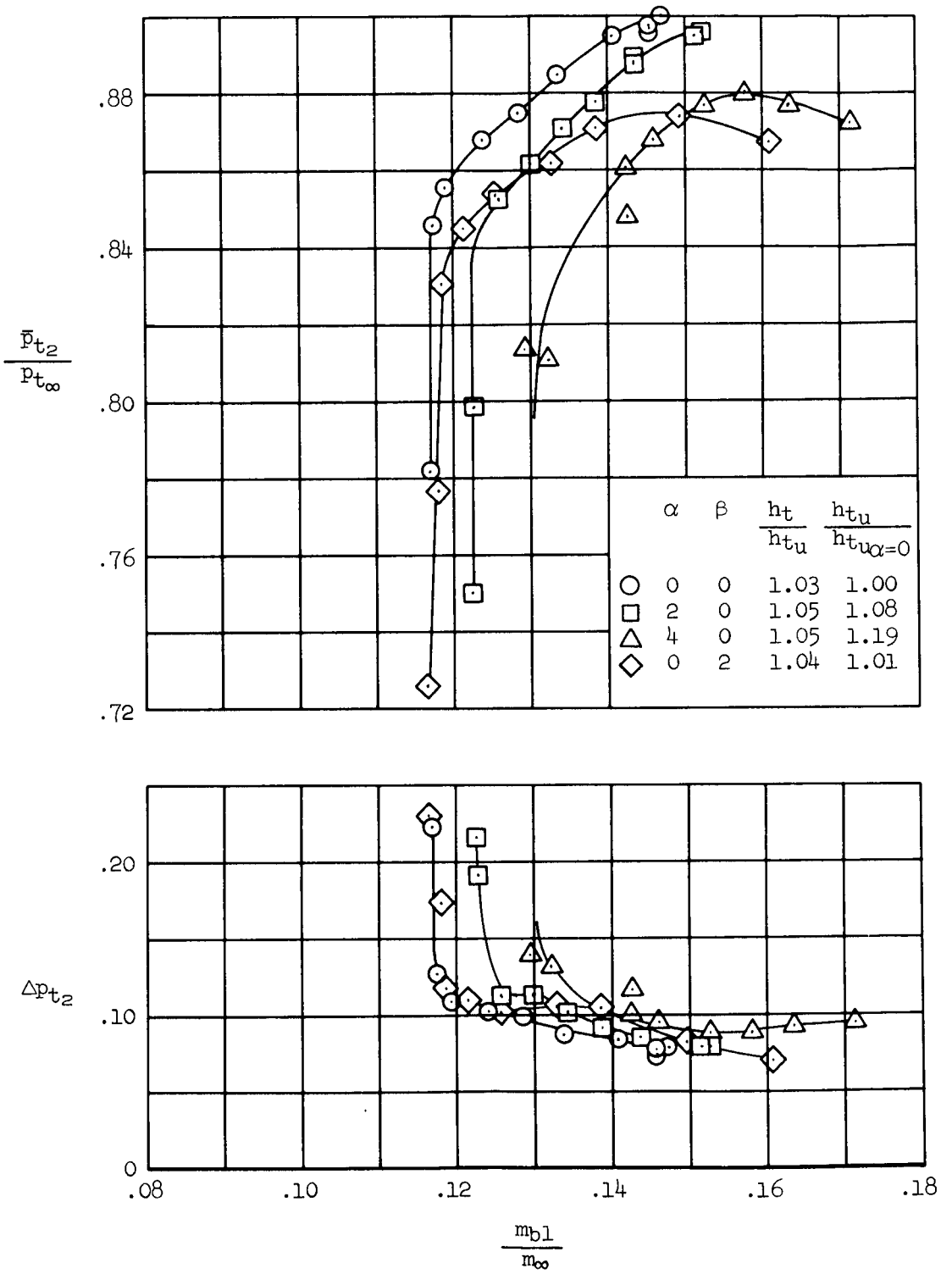

(a) $M_\infty = 3.00$

Figure 10.- The effect of inlet flow angularity on compression-efficiency parameters.

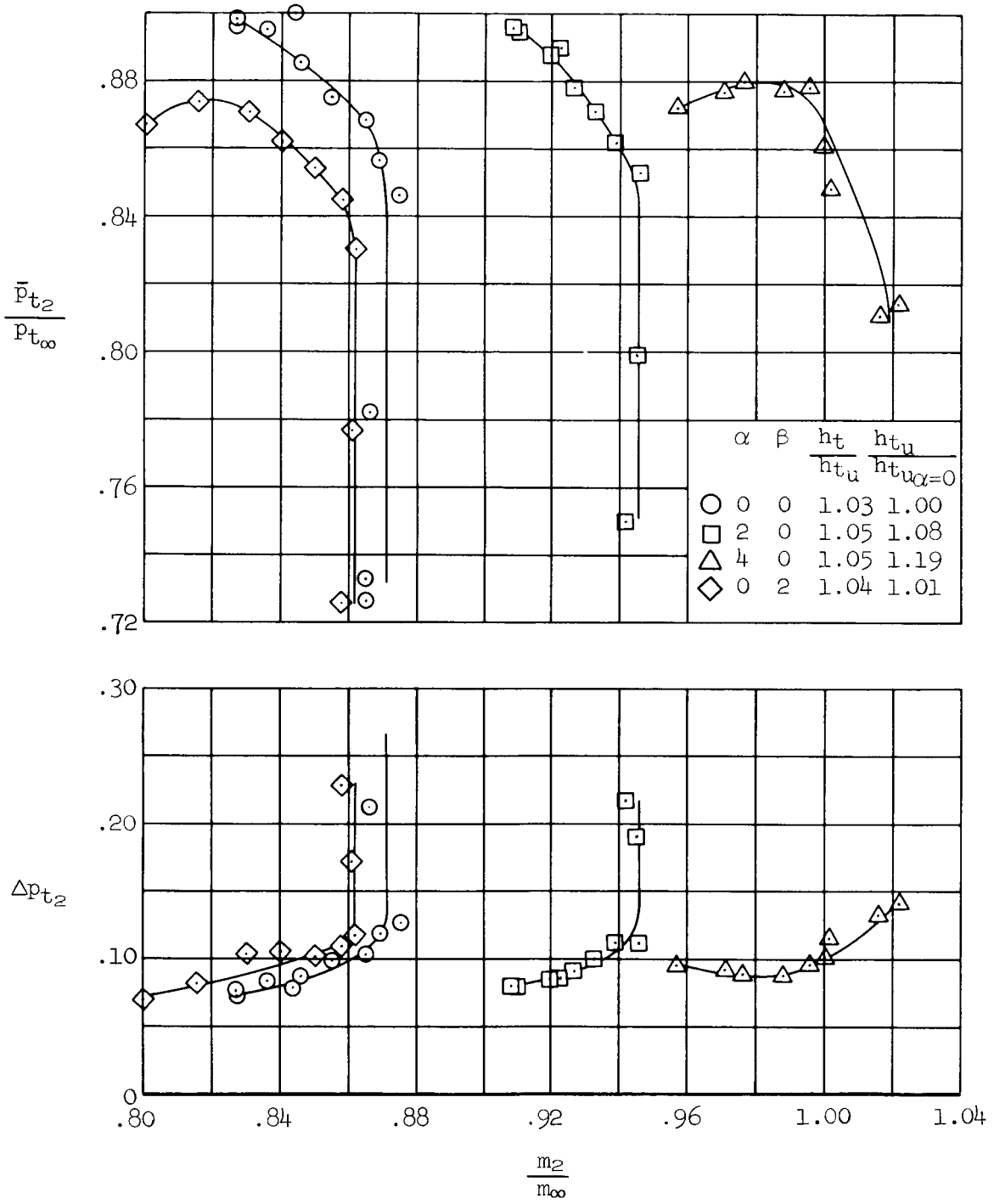

(a) $M_\infty = 3.00$ (concluded)

Figure 10.- Continued.

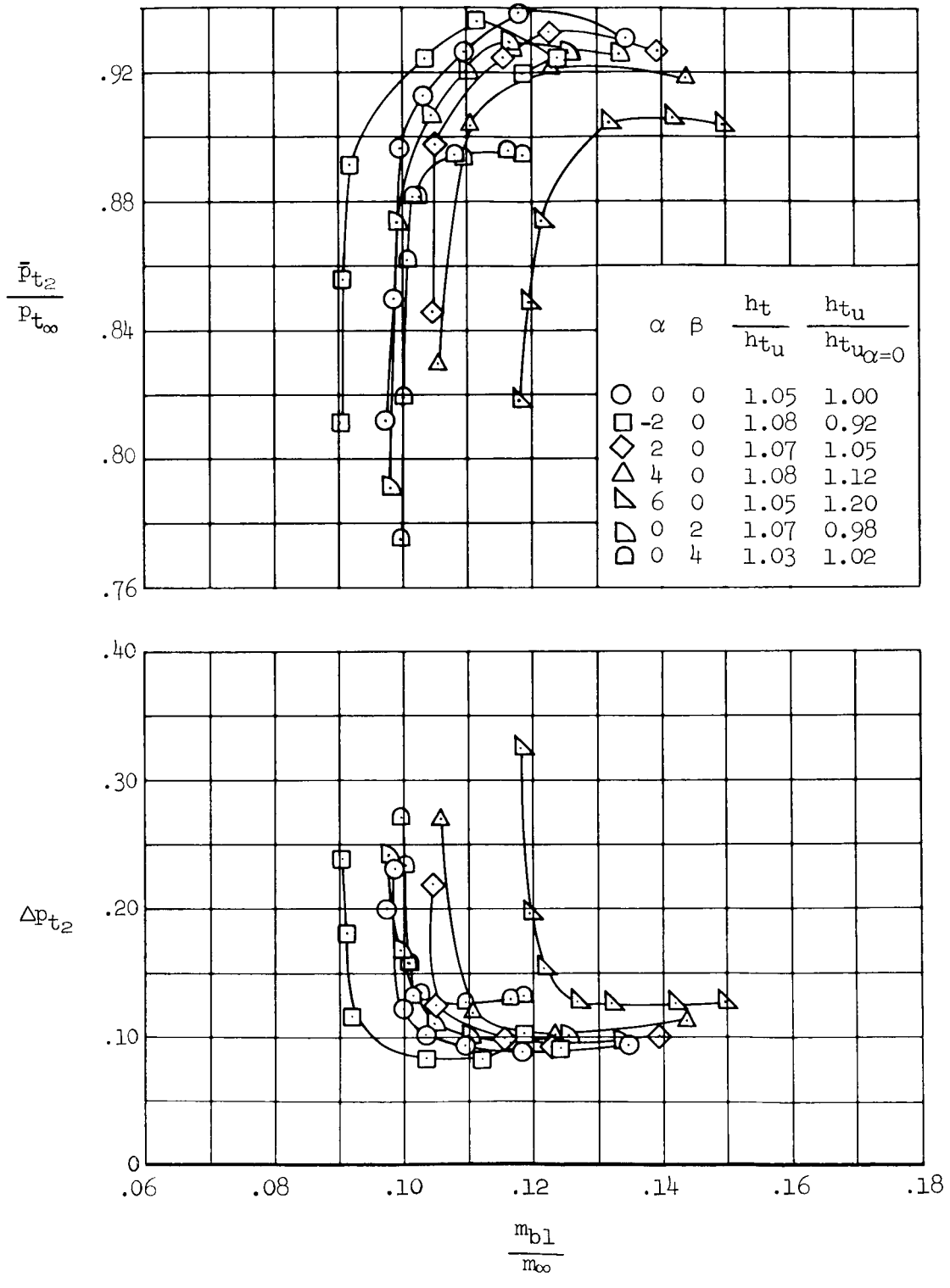

(b) $M_\infty = 2.50$

Figure 10.- Continued.

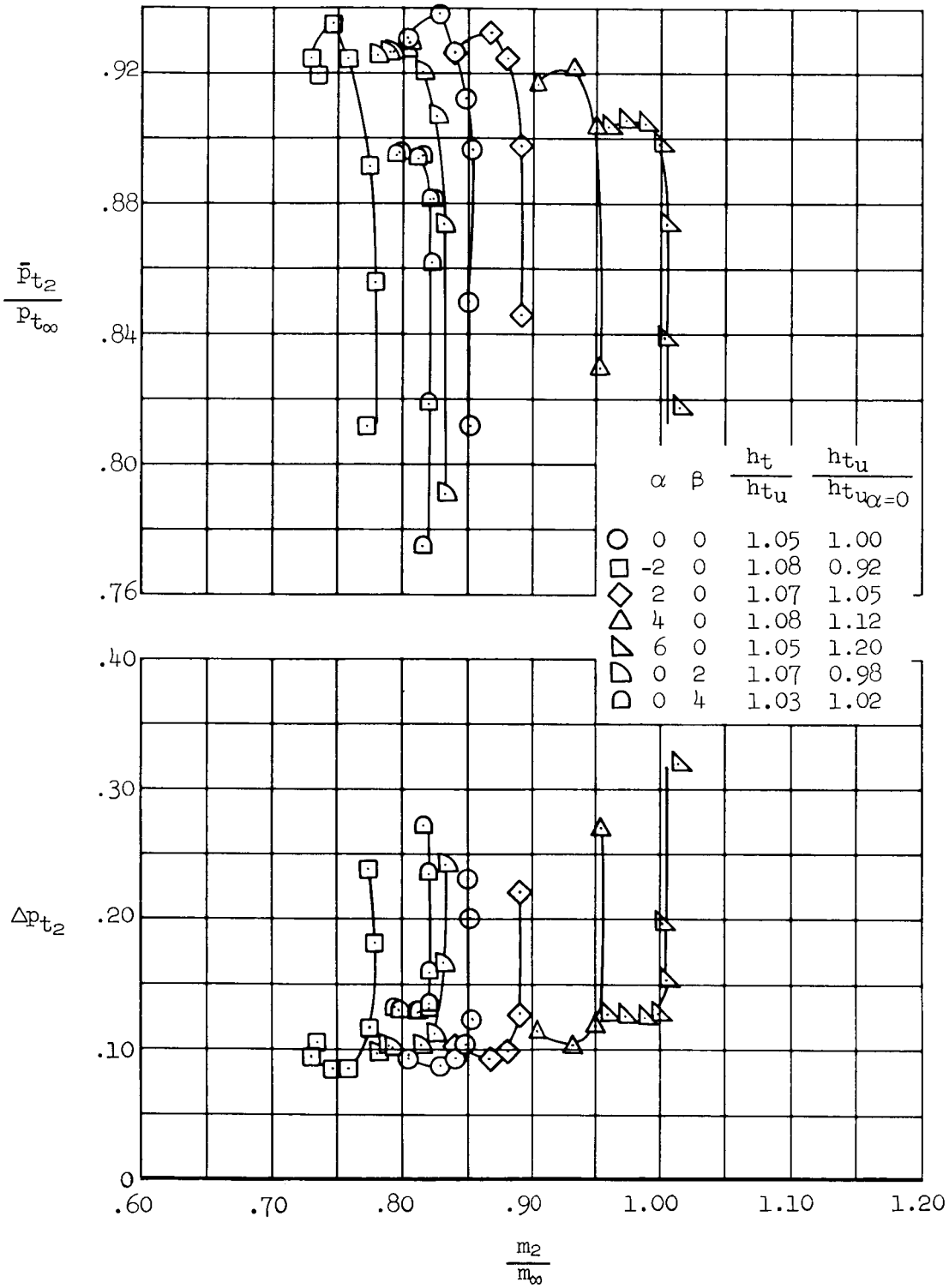

(b) $M_\infty = 2.50$ (concluded)

Figure 10.- Continued.

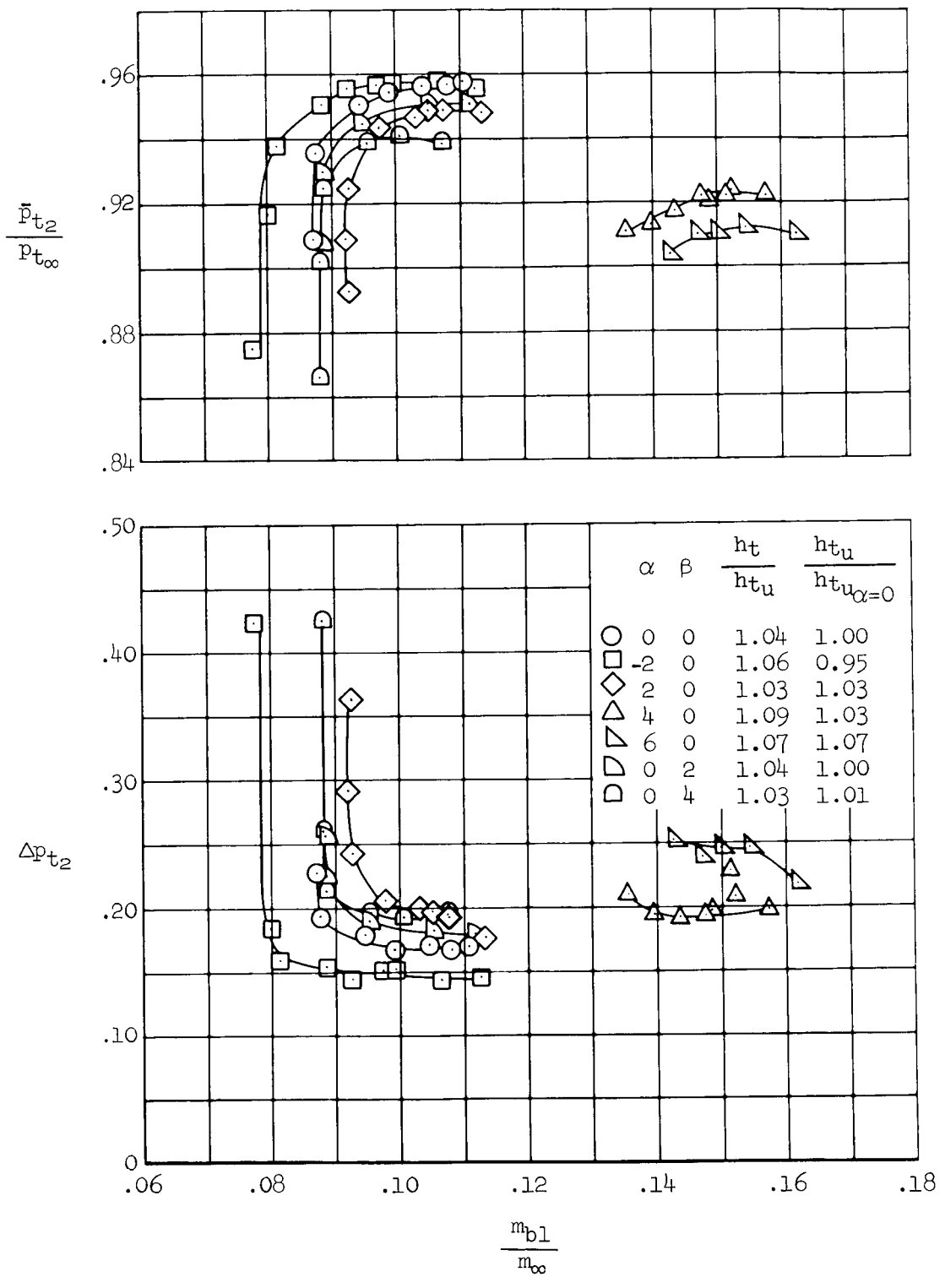

(c) $M_\infty = 2.00$

Figure 10.- Continued.

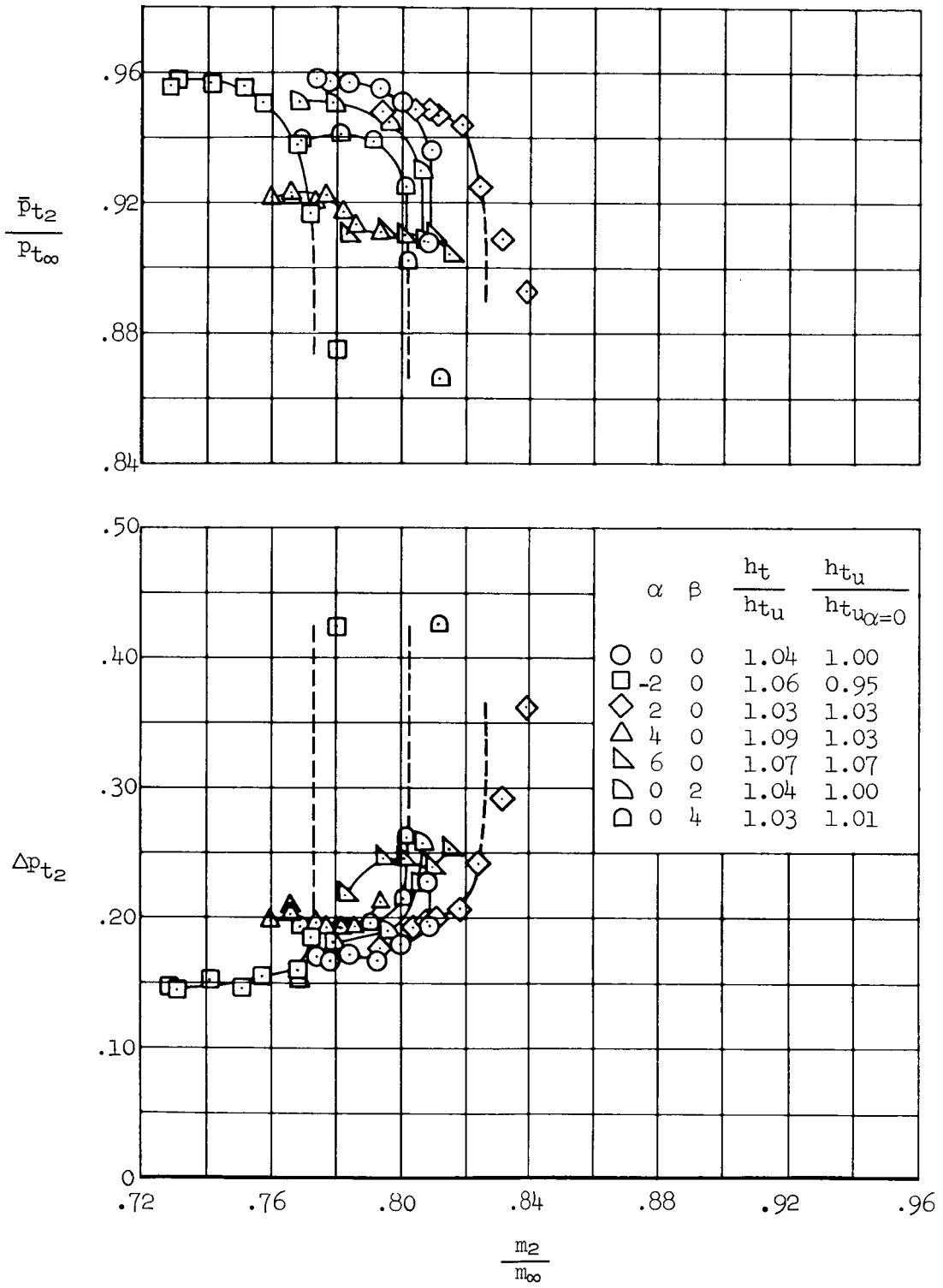

(c) $M_\infty = 2.00$ (concluded)

Figure 10.- Continued.

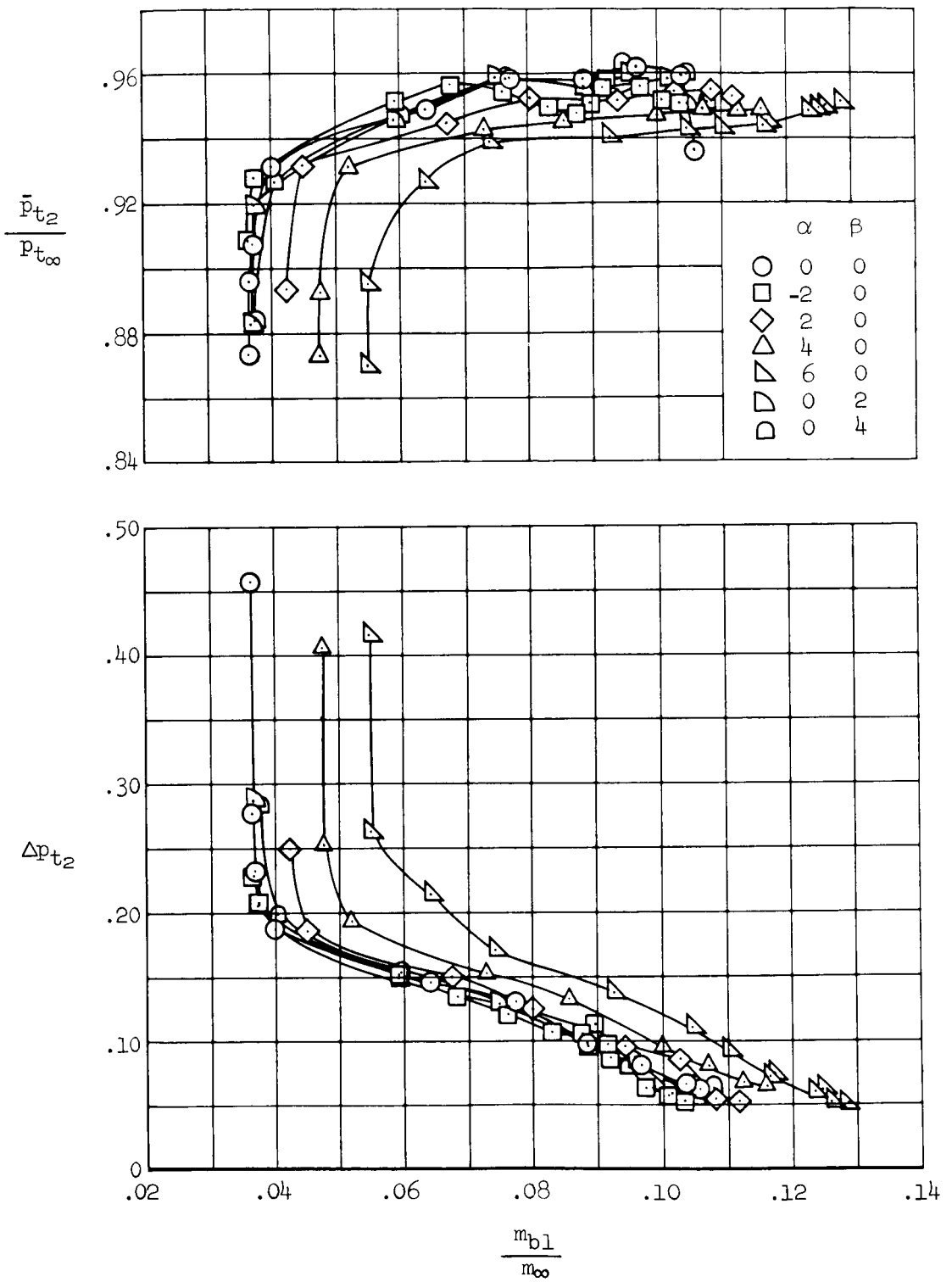

(d) $M_\infty = 1.55$

Figure 10.- Continued.

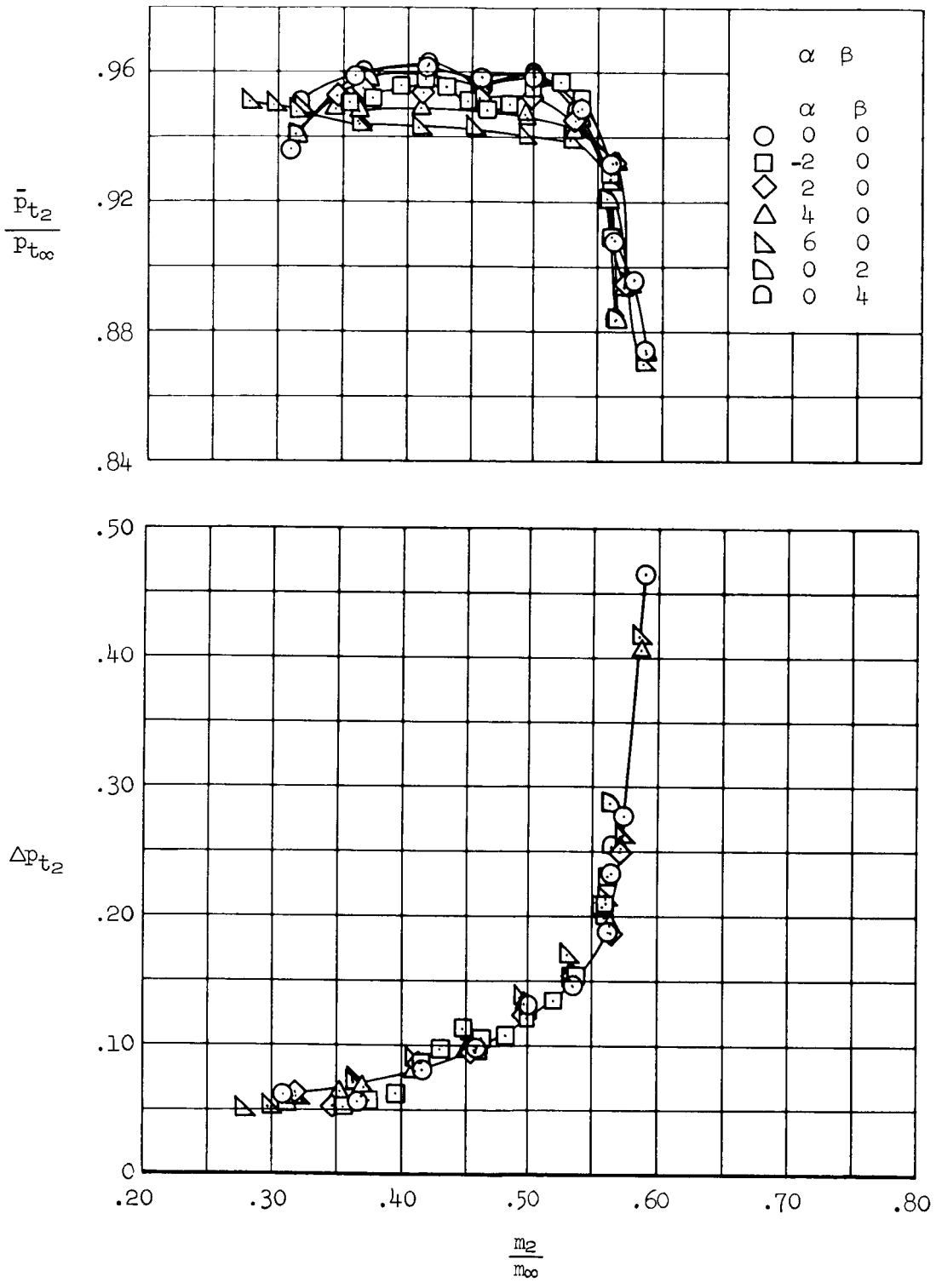

(d) $M_\infty = 1.55$ (concluded)

Figure 10.- Concluded.

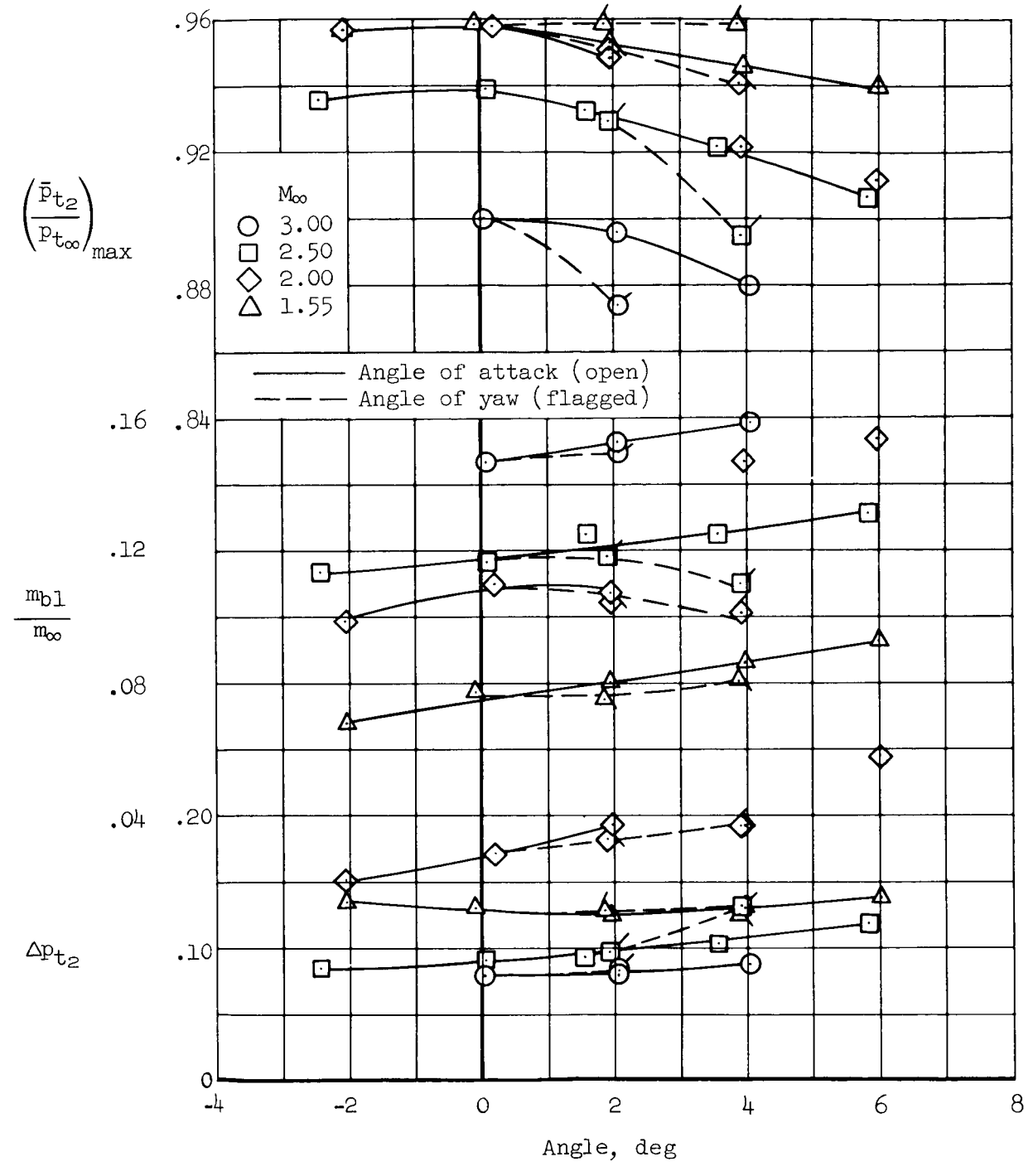

Figure 11.- The effect of angle of attack and angle of yaw on inlet compression-efficiency parameters for maximum total-pressure recovery.

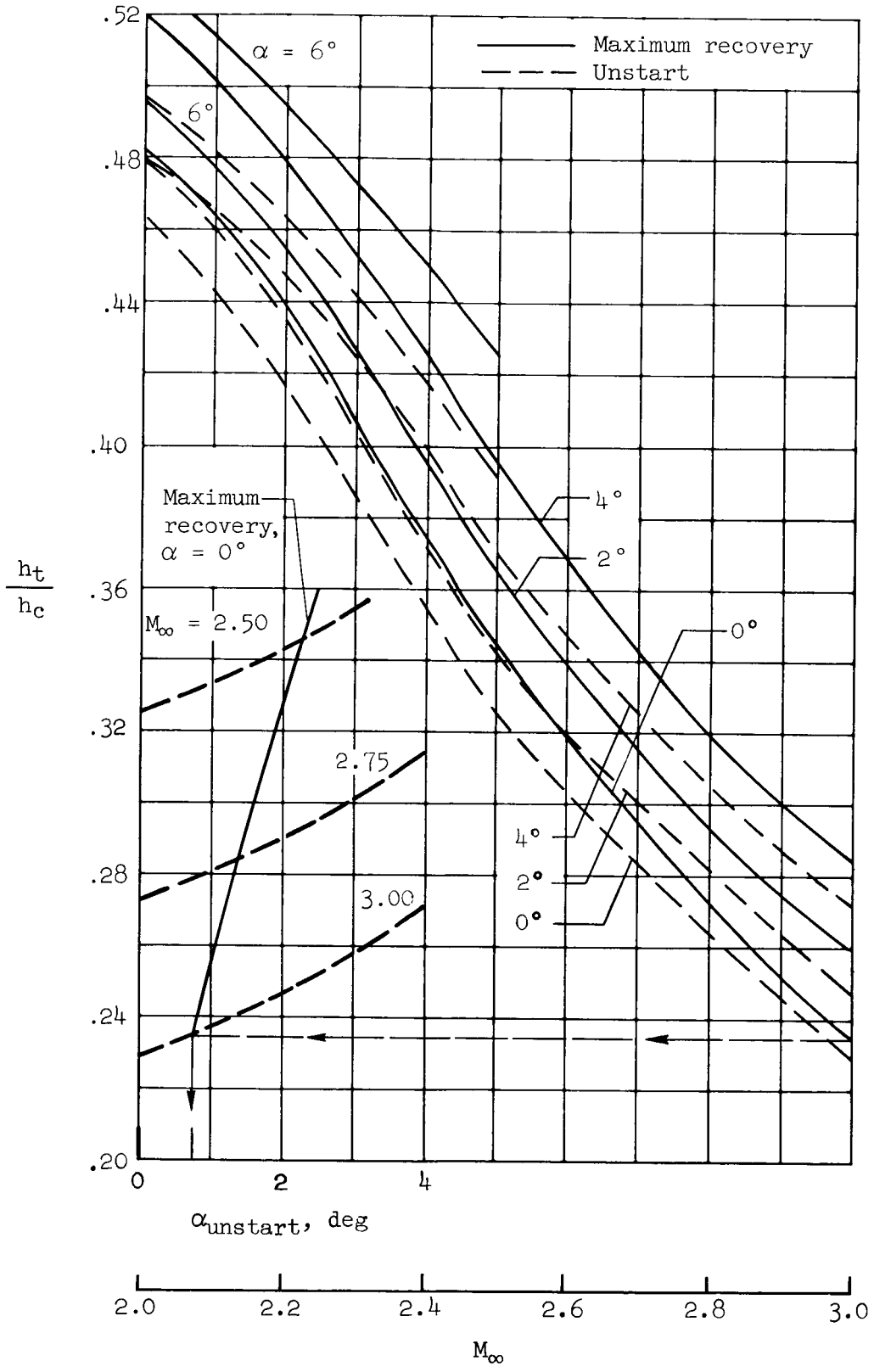

Figure 12.- The effect of Mach number on operating throat height requirements.

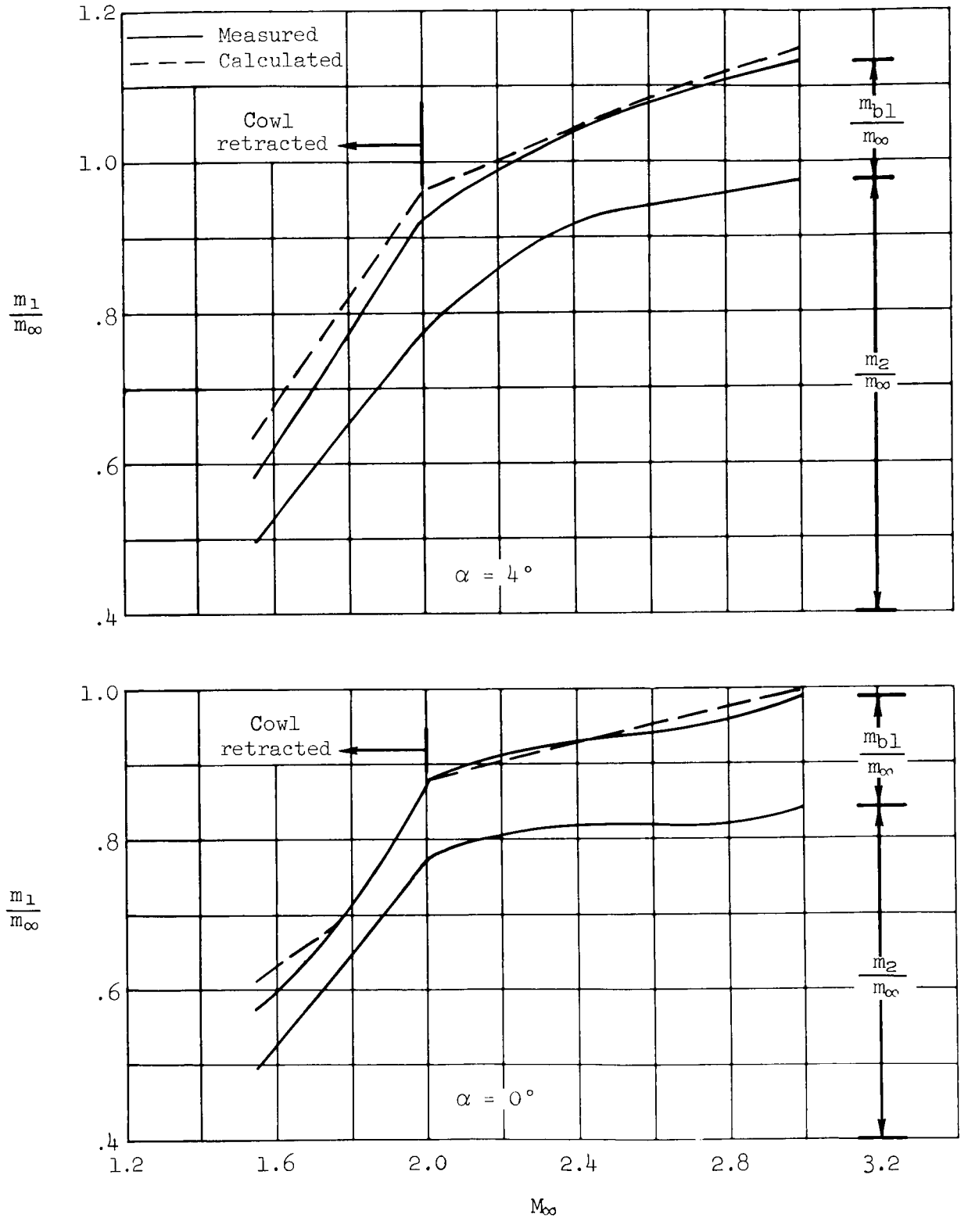

Figure 13.- The effect of Mach number on inlet mass-flow ratio for maximum total-pressure recovery.

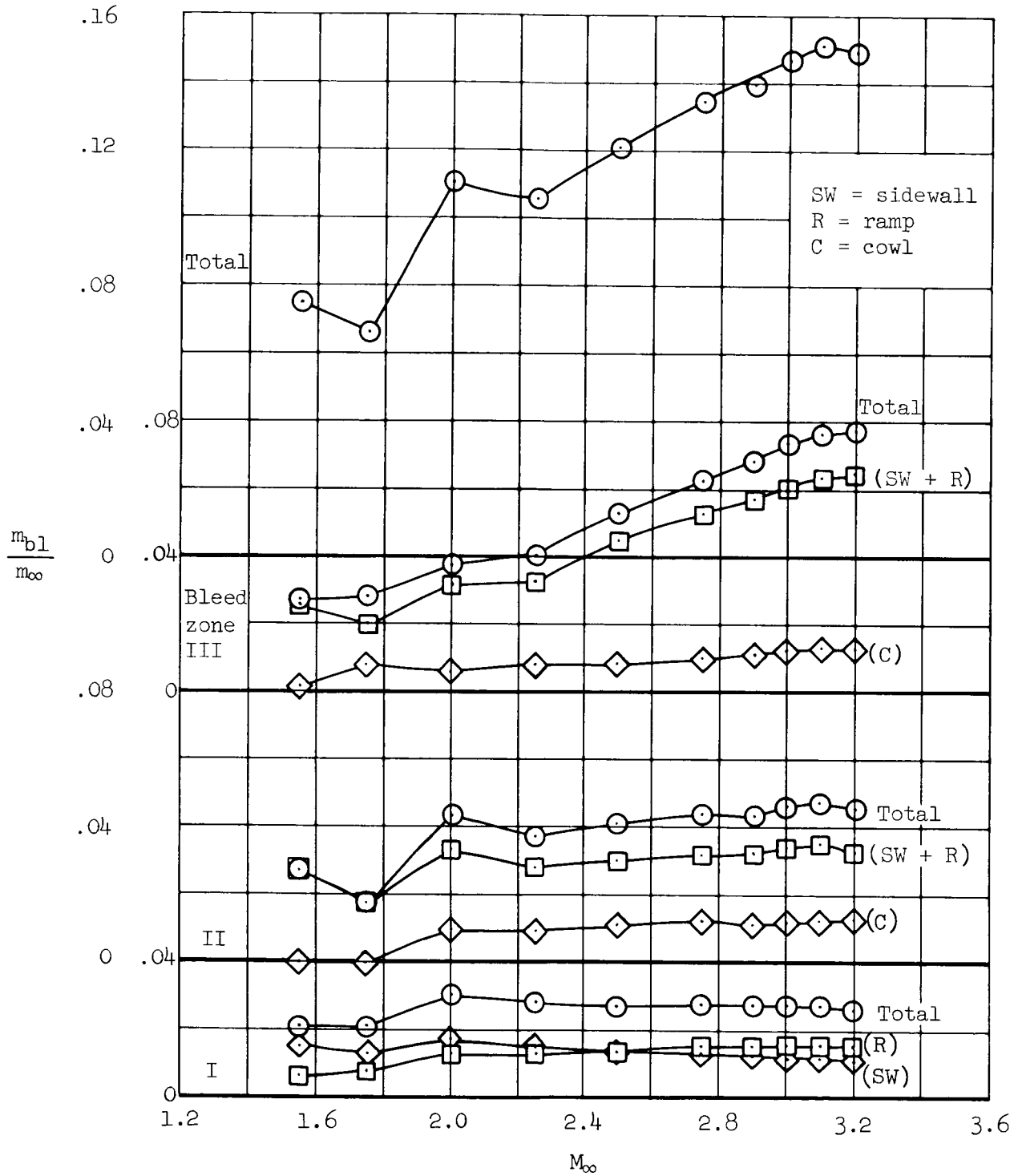

Figure 14.- The effect of Mach number on composite bleed mass-flow ratio characteristics for maximum total-pressure recovery; $\alpha = 0°$, $\beta = 0°$.

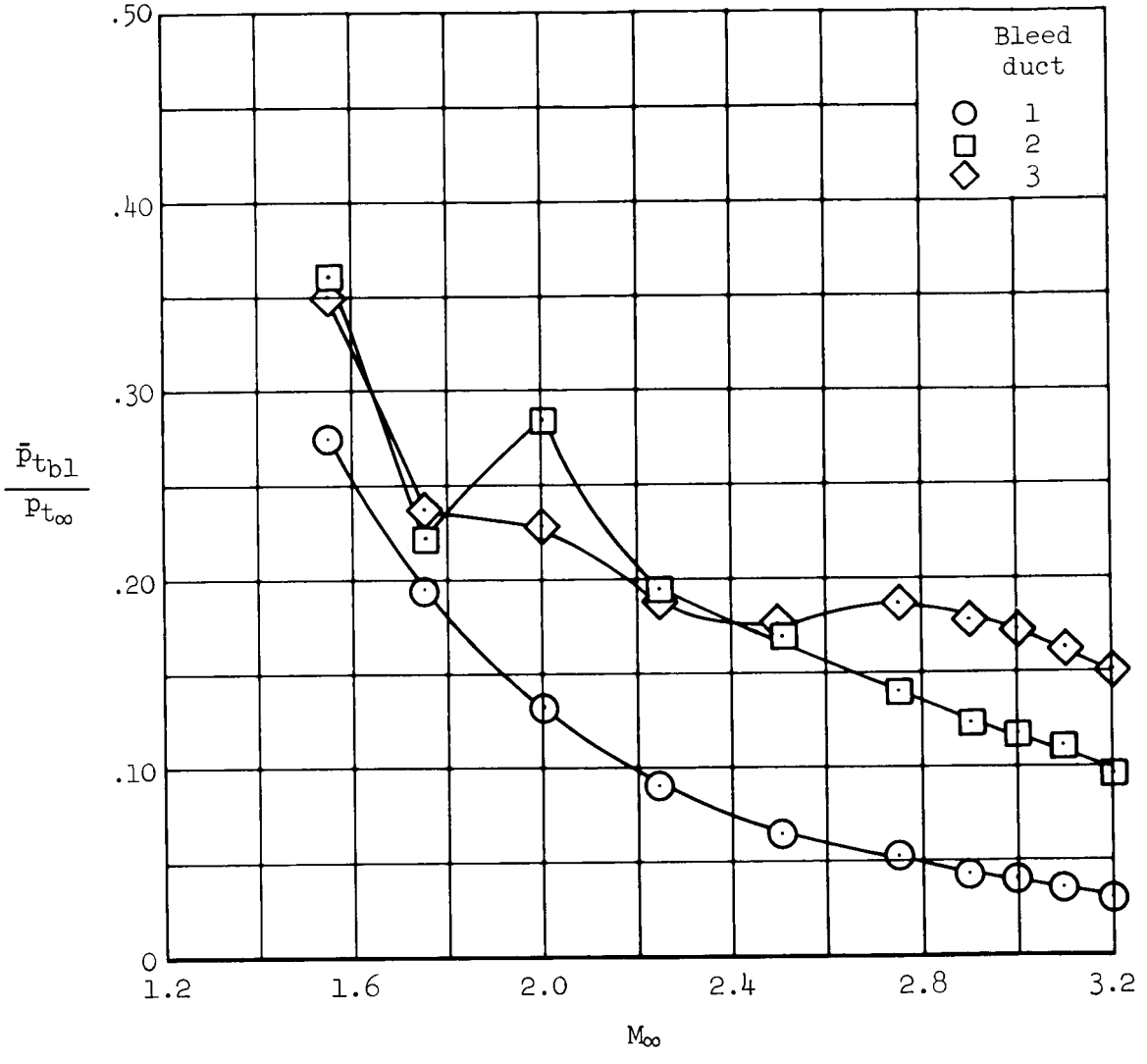

Figure 15.- The effect of Mach number on bleed duct total-pressure ratio for maximum engine-face recovery; $\alpha = 0°$, $\beta = 0°$.

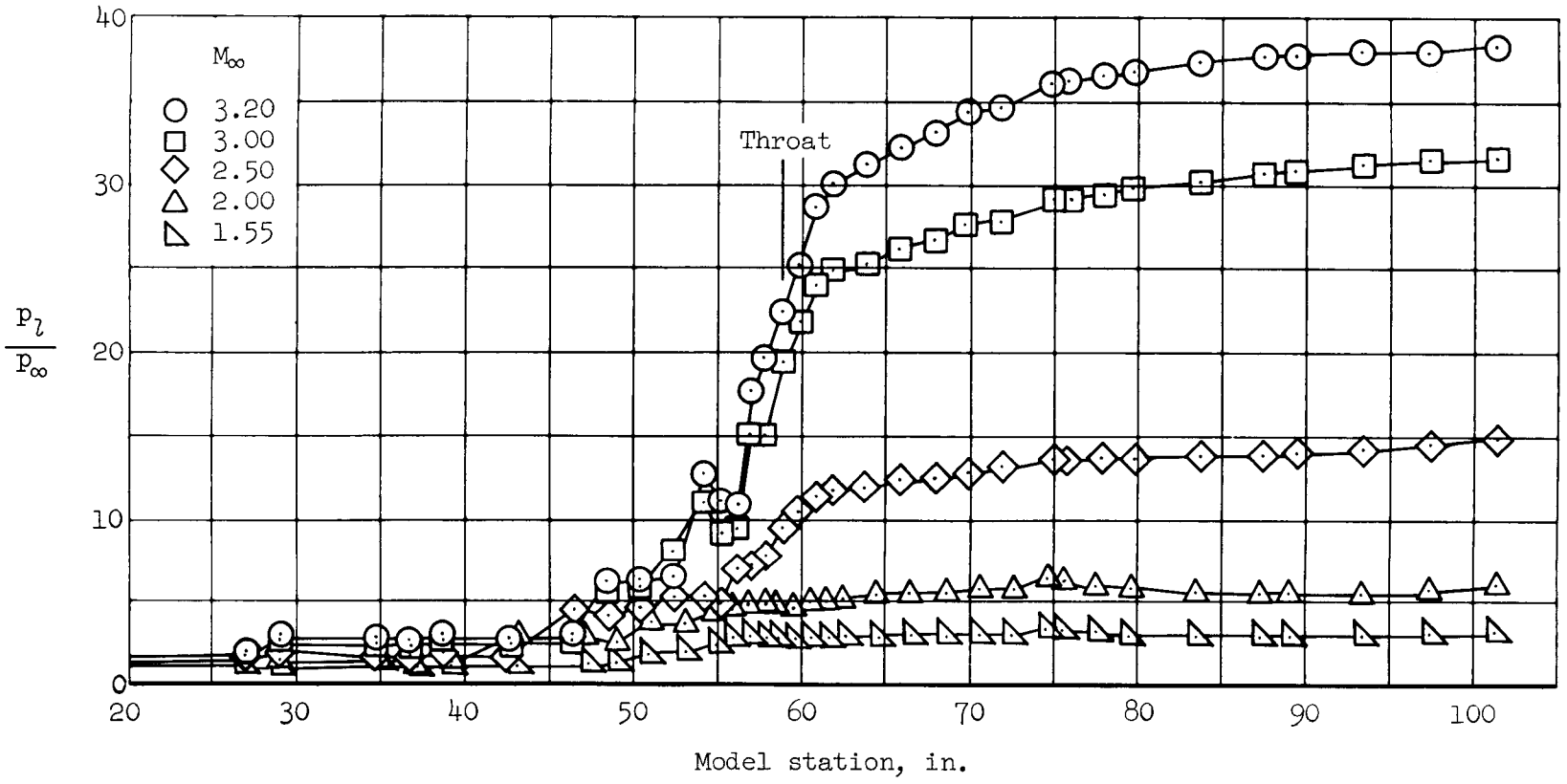

(a) Ramp

Figure 16.- Static pressure characteristics at maximum engine-face recovery; $\alpha = 0°$, $\beta = 0°$.

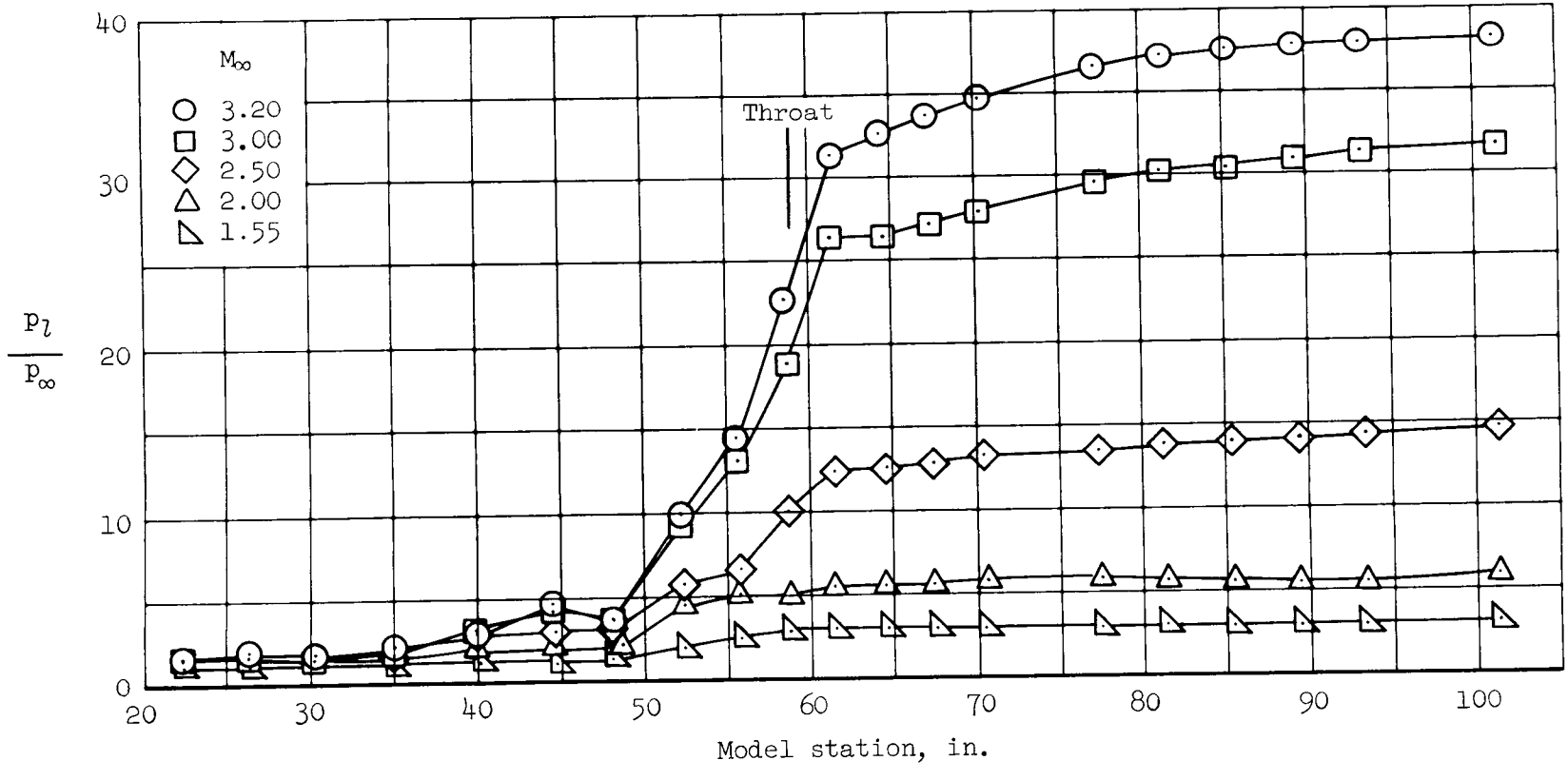

(b) Sidewall

Figure 16.- Continued.

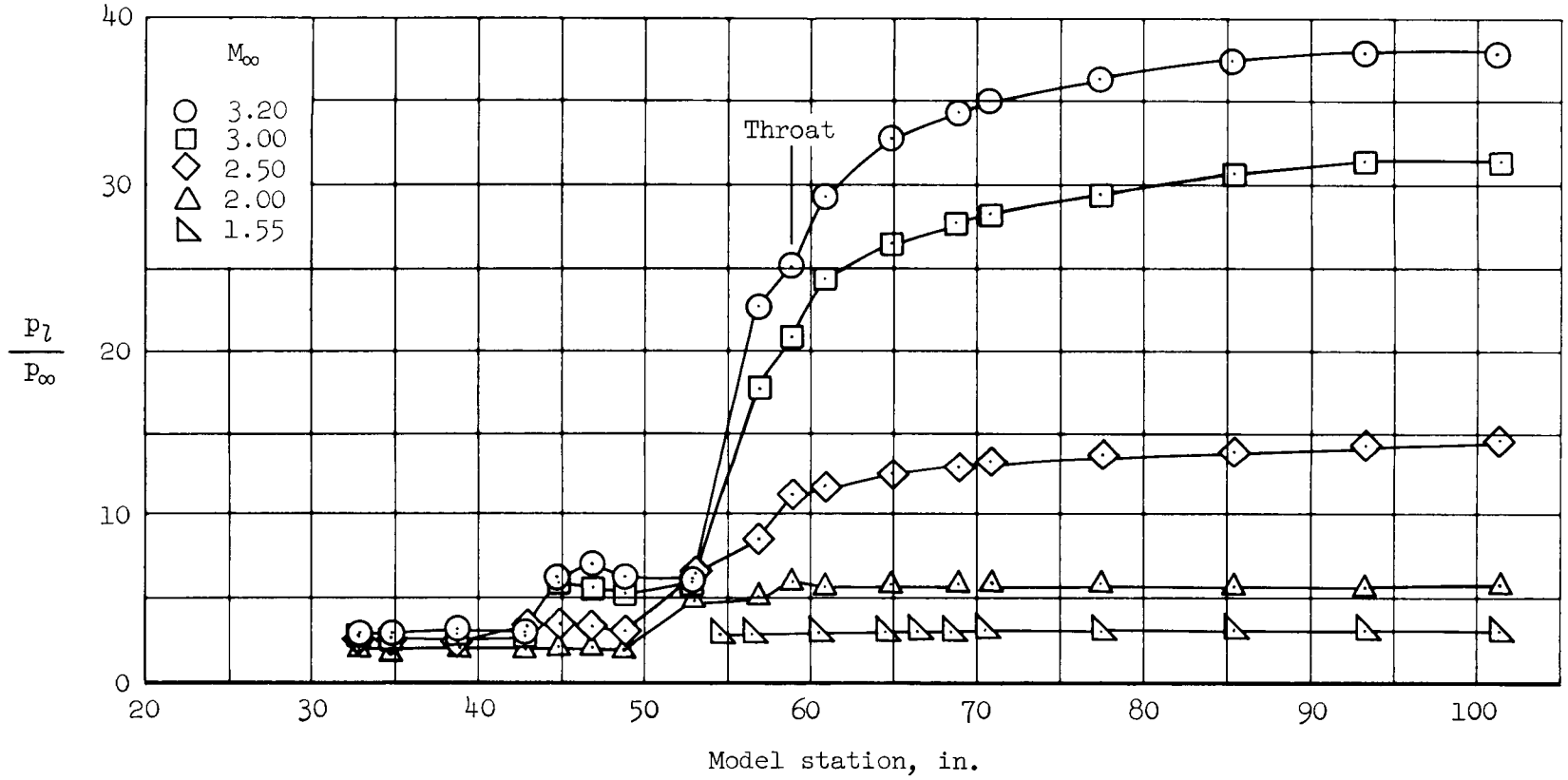

(c) Cowl

Figure 16.- Concluded.

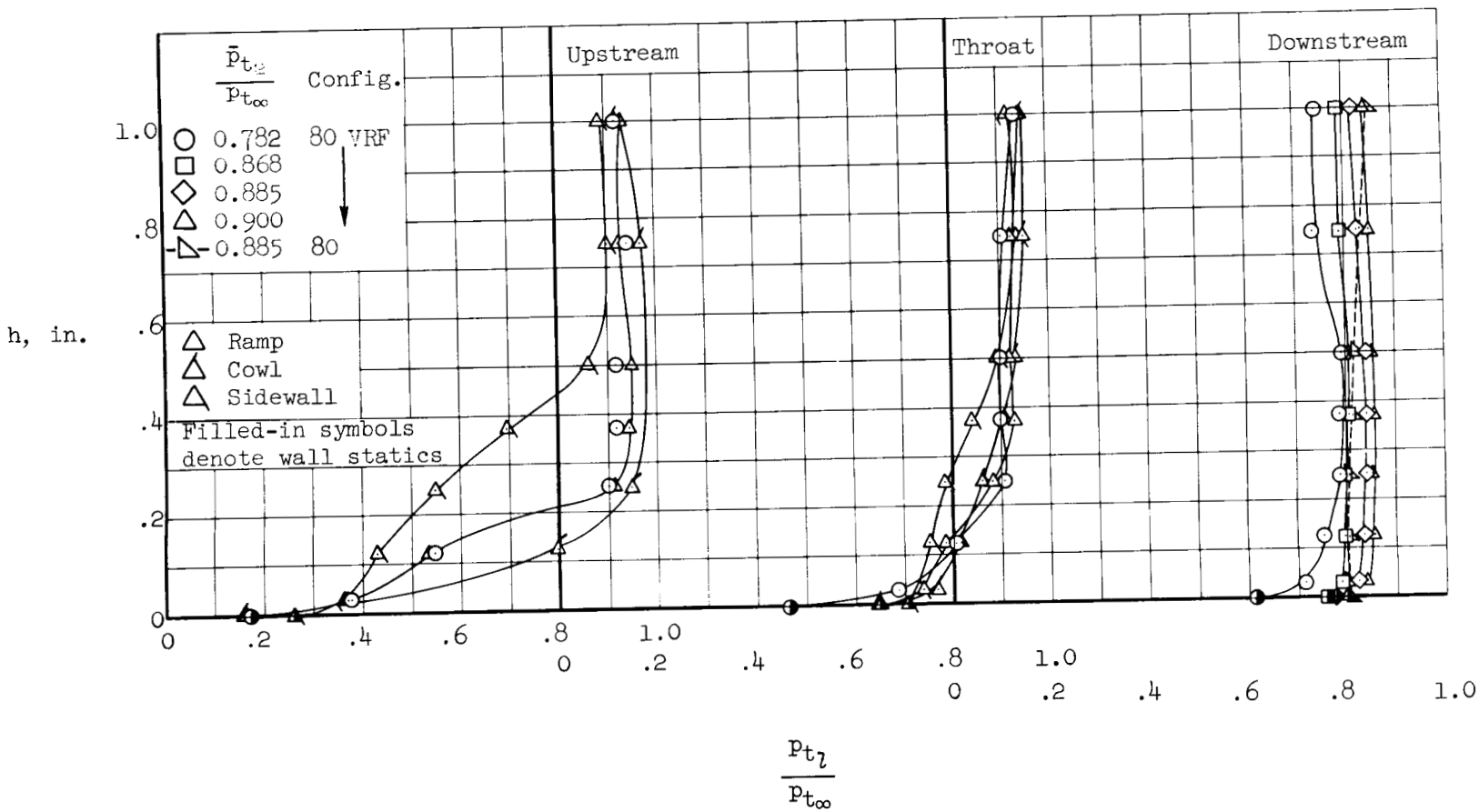

(a) $M_\infty = 3.00$

Figure 17.- Boundary-layer total-pressure profiles at three duct locations; $\alpha = 0°$, $\beta = 0°$.

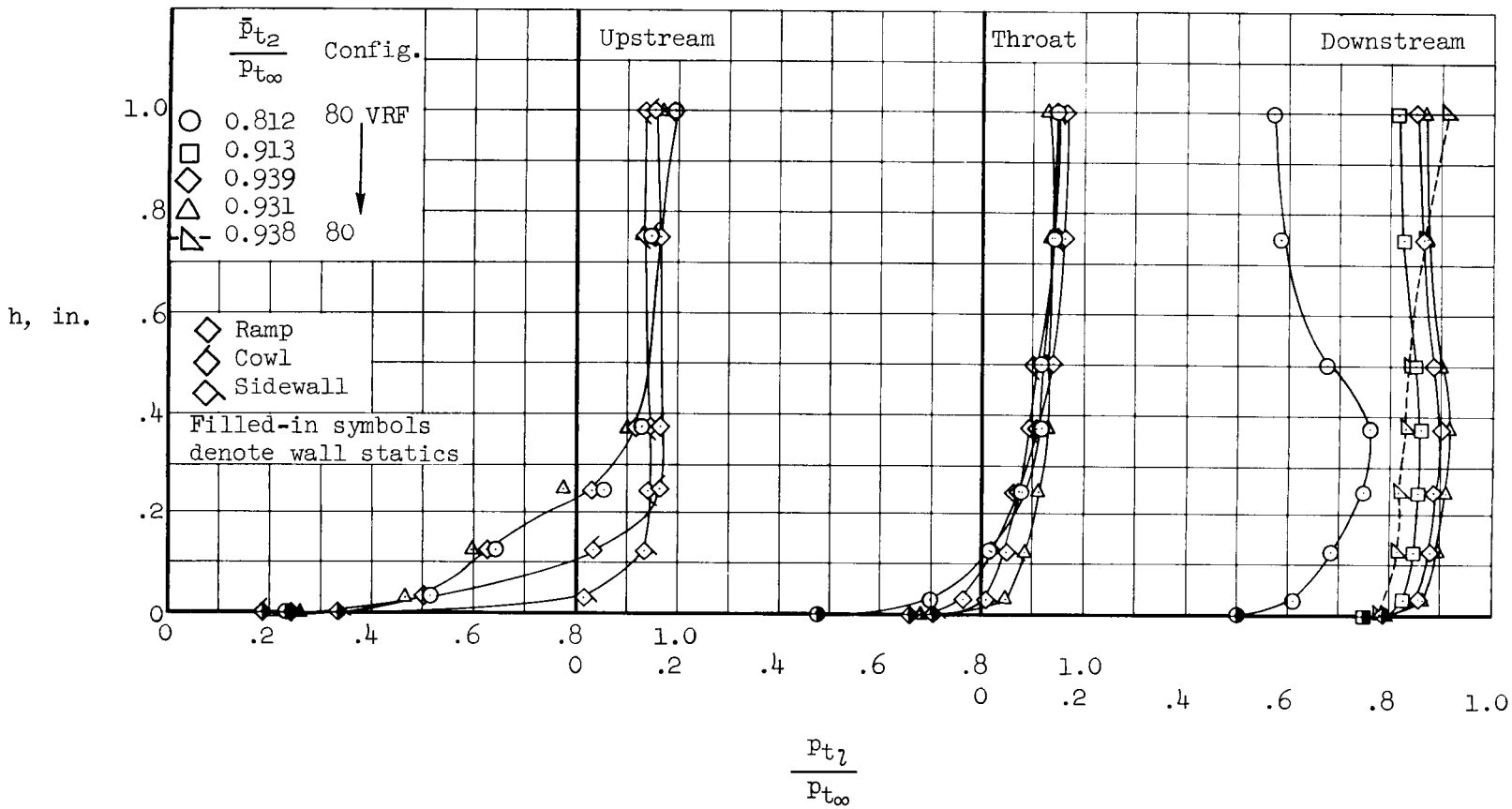

(b) $M_\infty = 2.50$

Figure 17.- Continued.

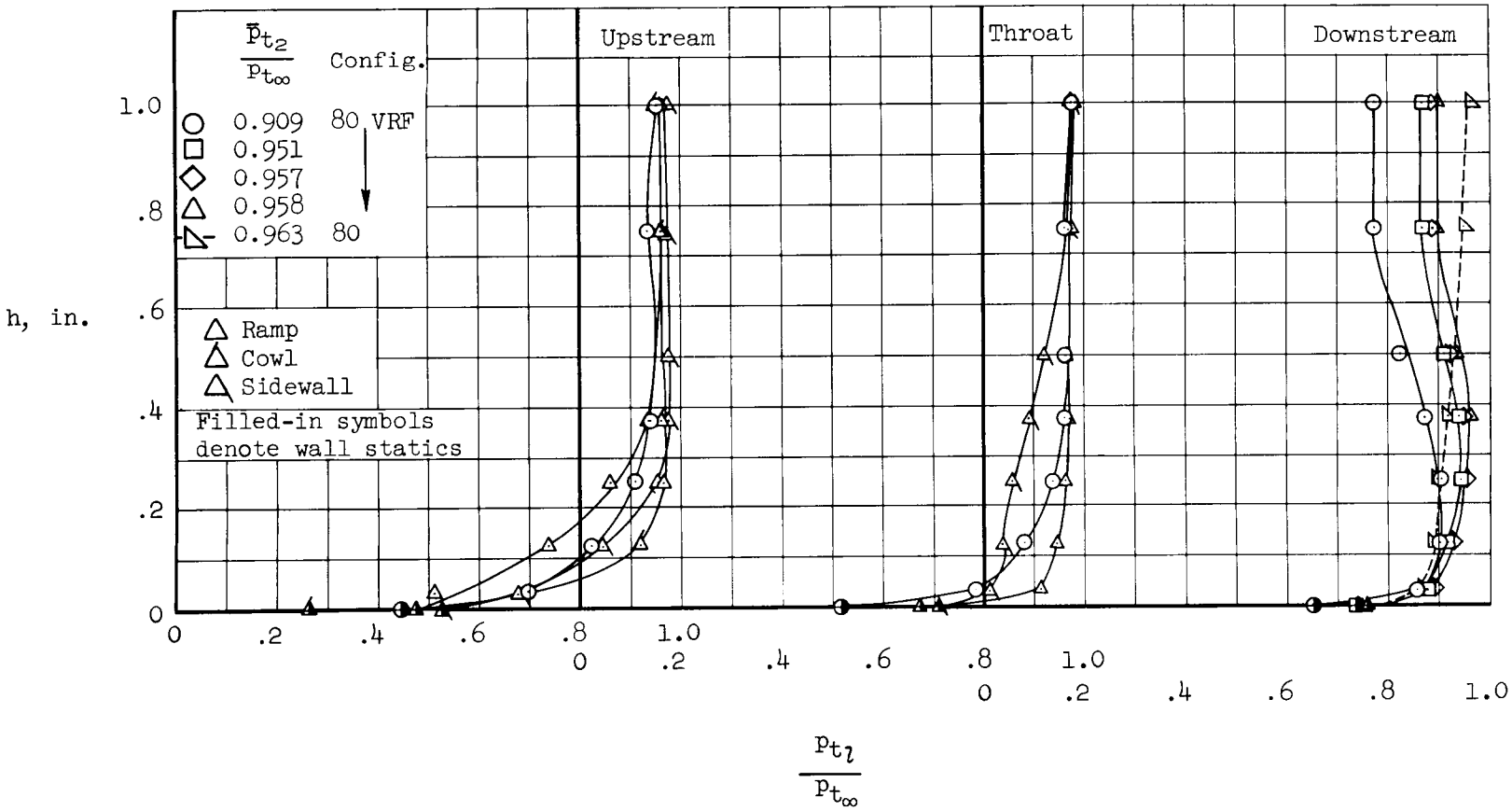

(c) $M_\infty = 2.00$

Figure 17.- Continued.

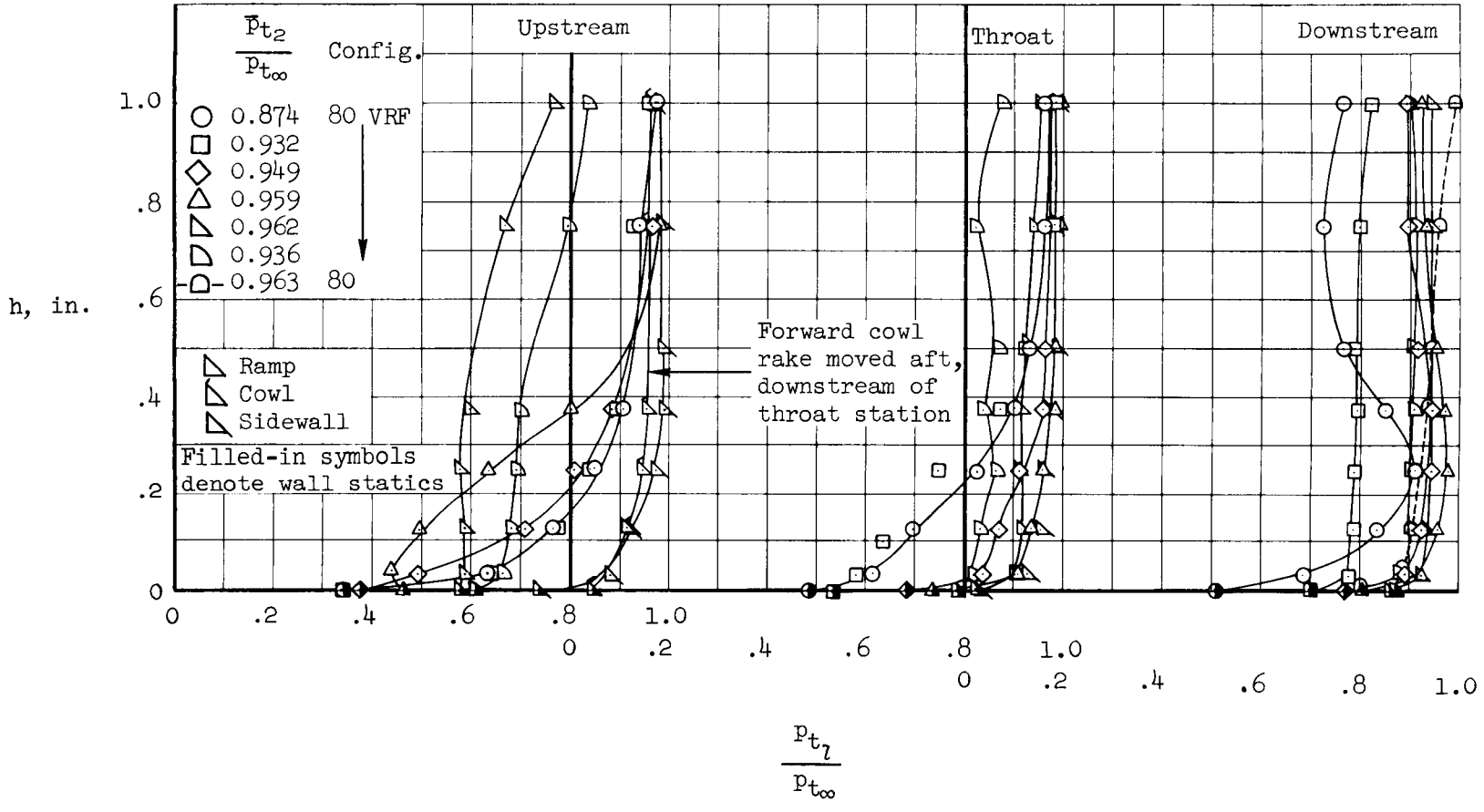

(d) $M_\infty = 1.55$

Figure 17.- Concluded.

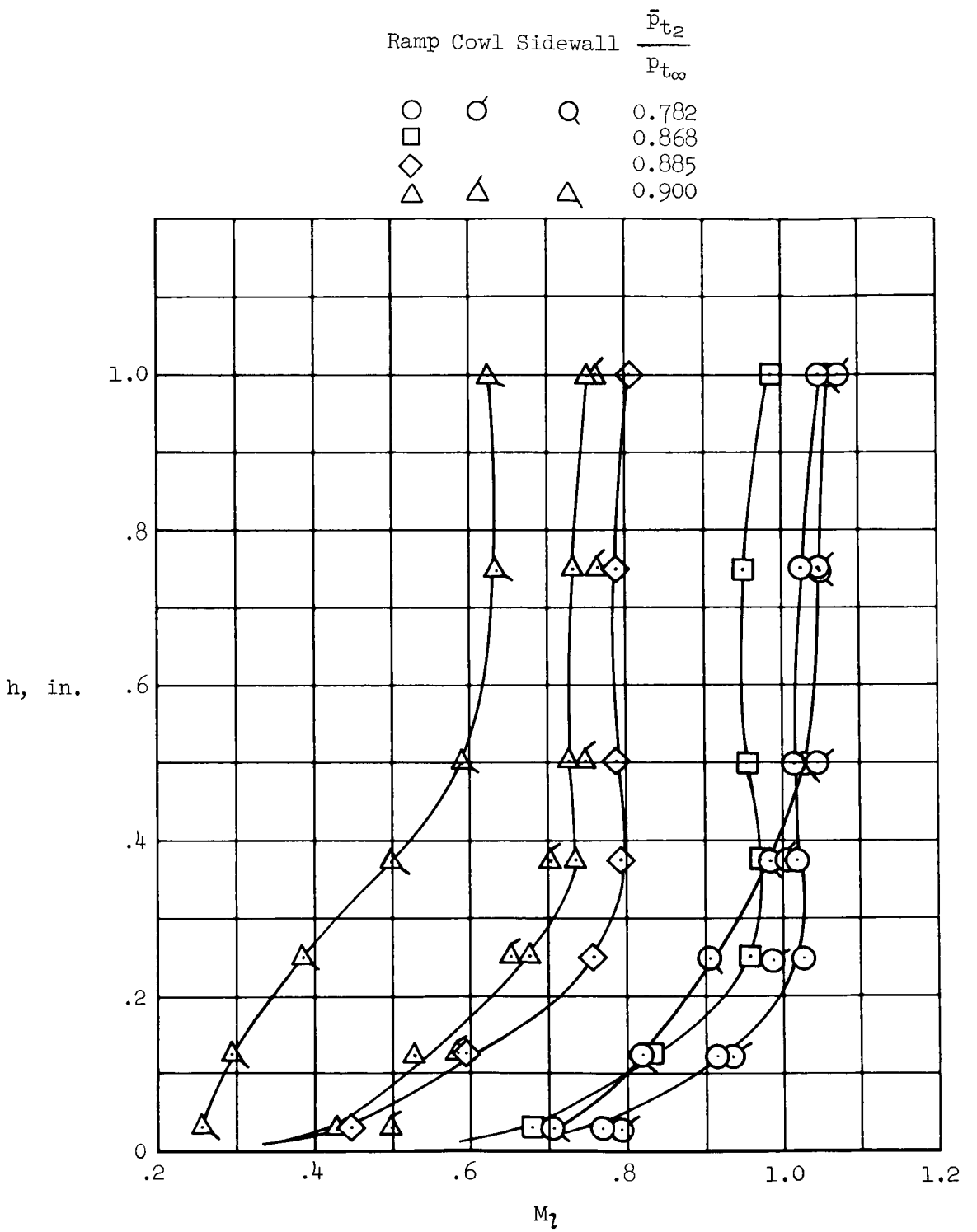

(a) $M_\infty = 3.00$

Figure 18.- Boundary-layer Mach number profiles at the throat location; $\alpha = 0°$, $\beta = 0°$.

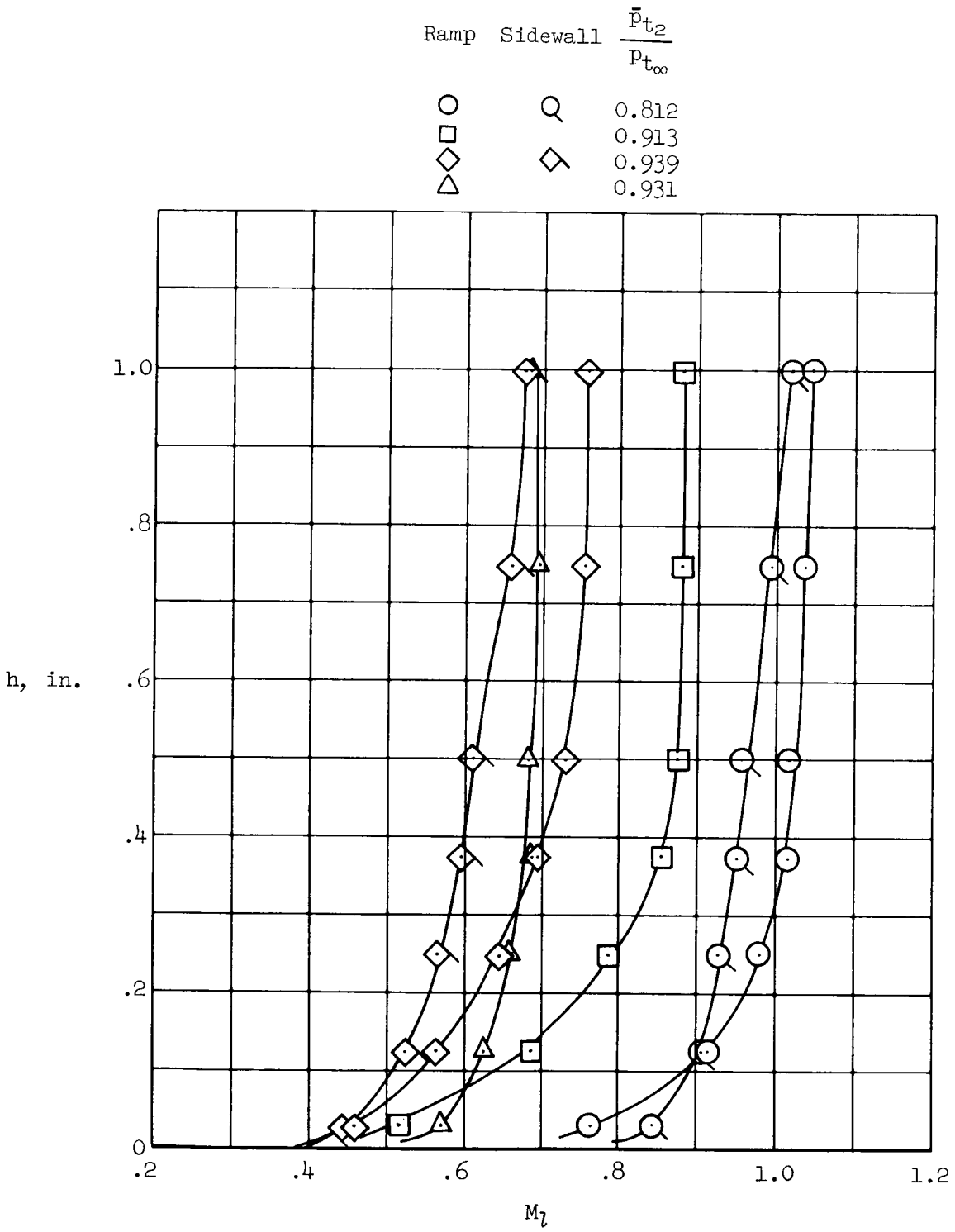

(b) $M_\infty = 2.50$

Figure 18.- Continued.

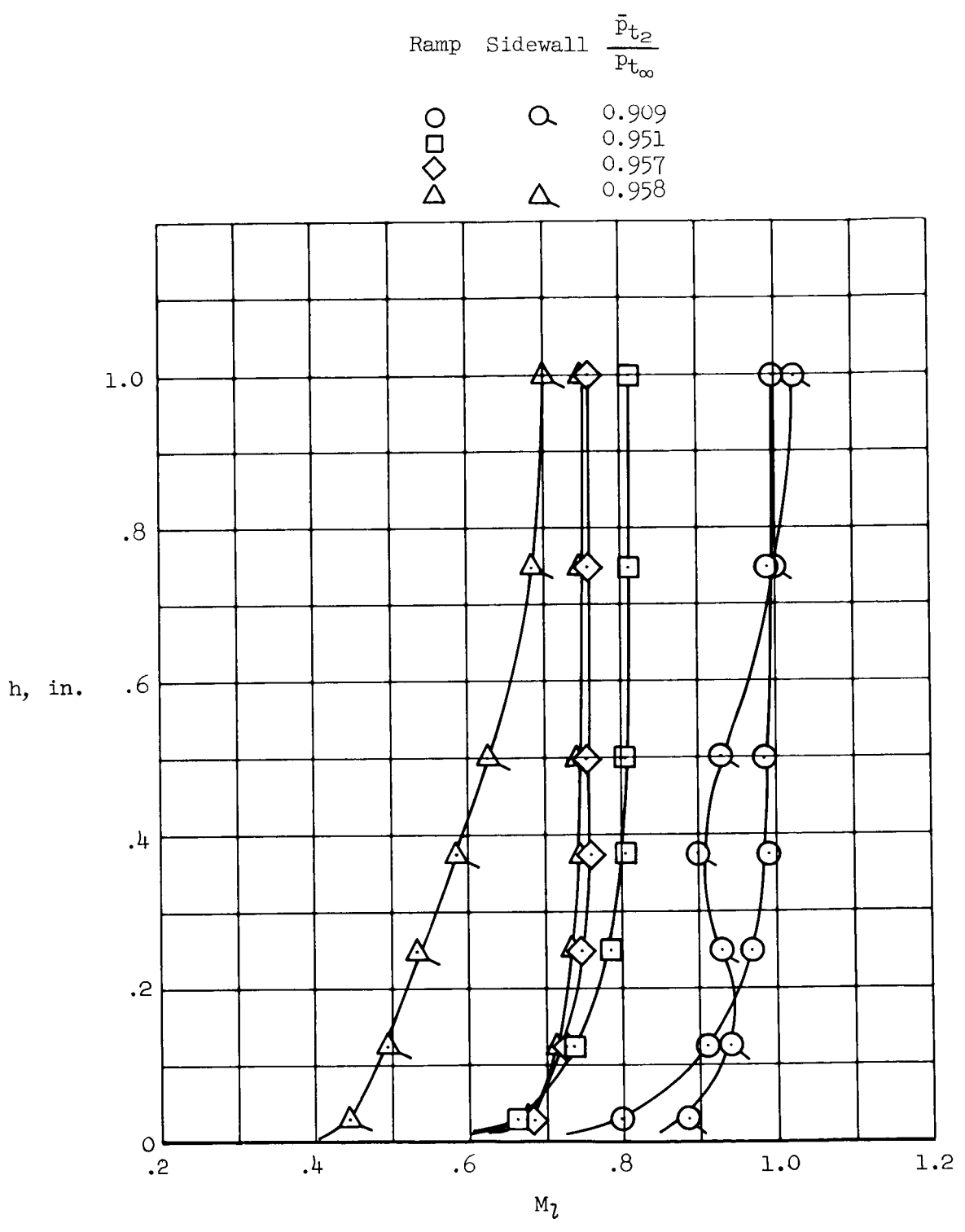

(c) $M_\infty = 2.00$

Figure 18.- Continued.

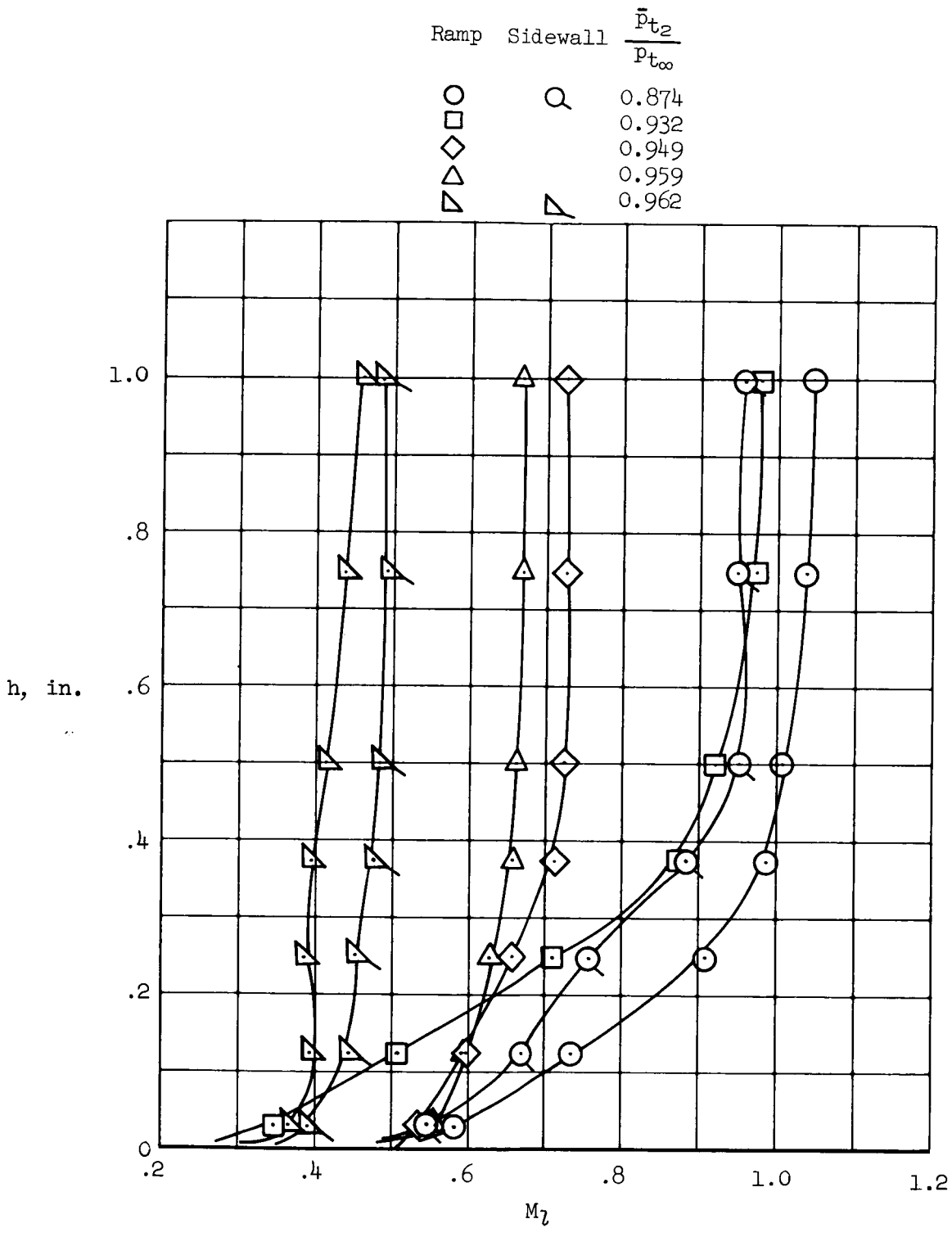

(d) $M_\infty = 1.55$

Figure 18.- Concluded.

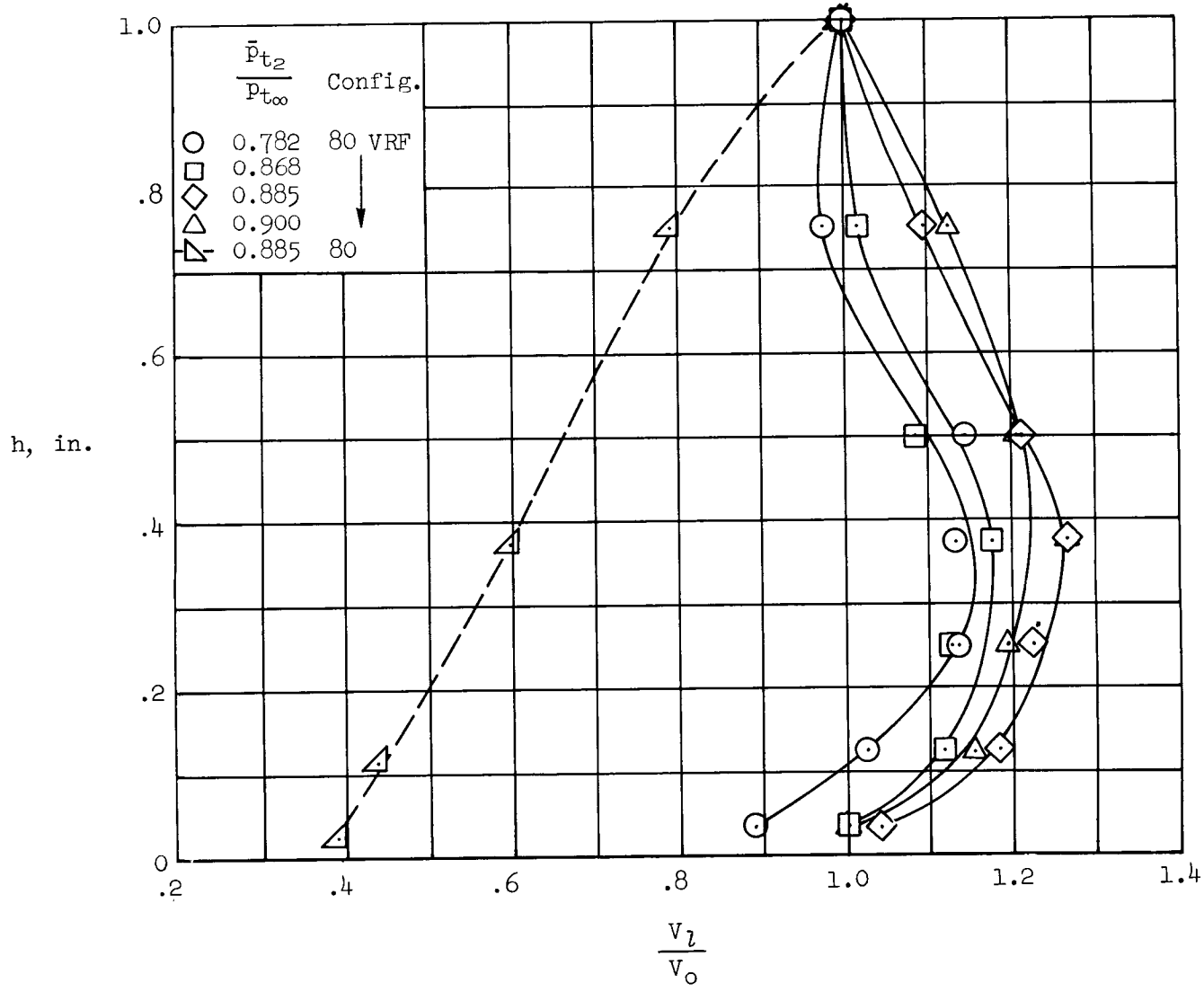

(a) $M_\infty = 3.00$

Figure 19.- Boundary-layer velocity profiles at the downstream ramp location; $\alpha = 0°$, $\beta = 0°$.

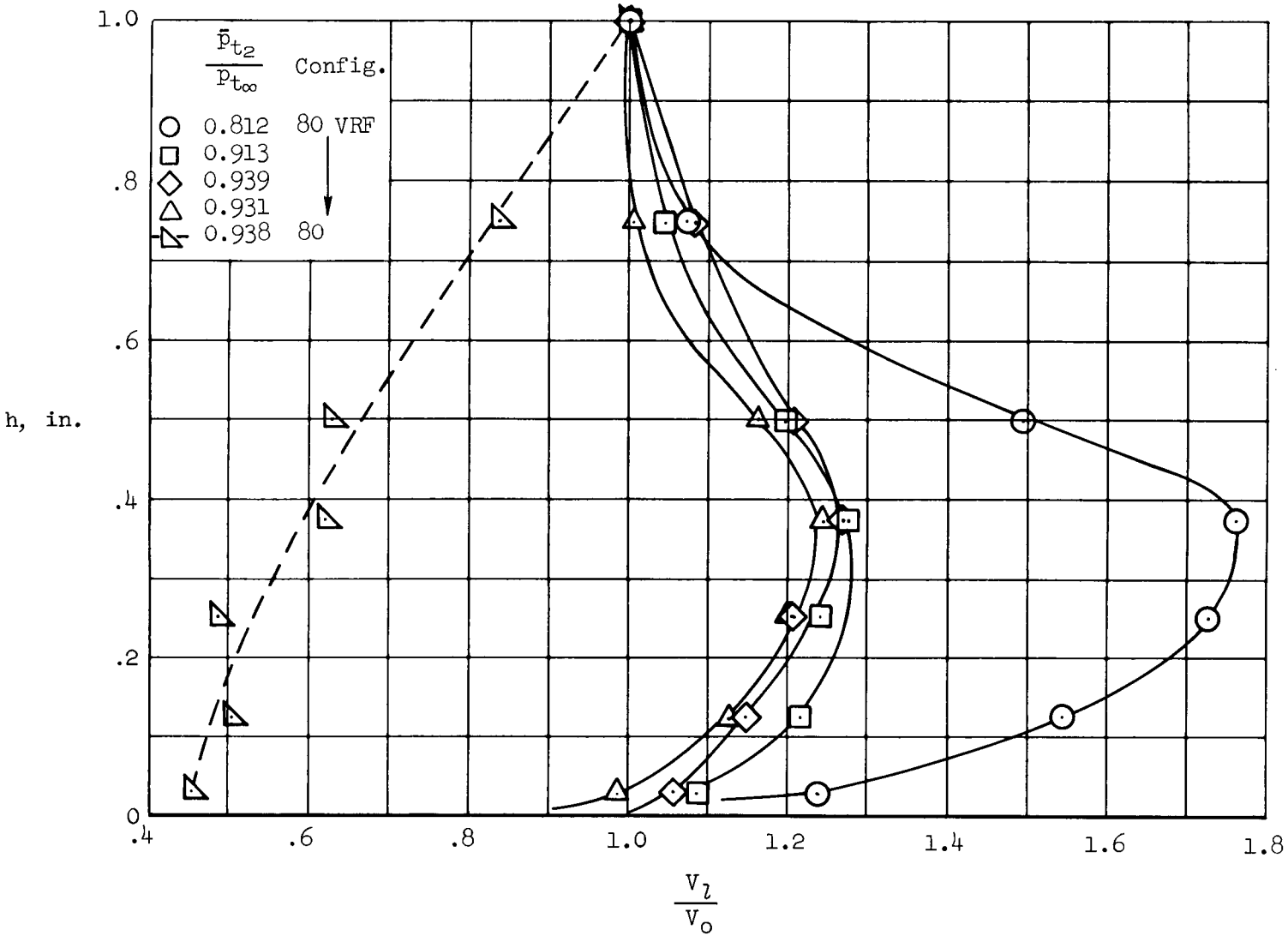

(b) $M_\infty = 2.50$

Figure 19.- Continued.

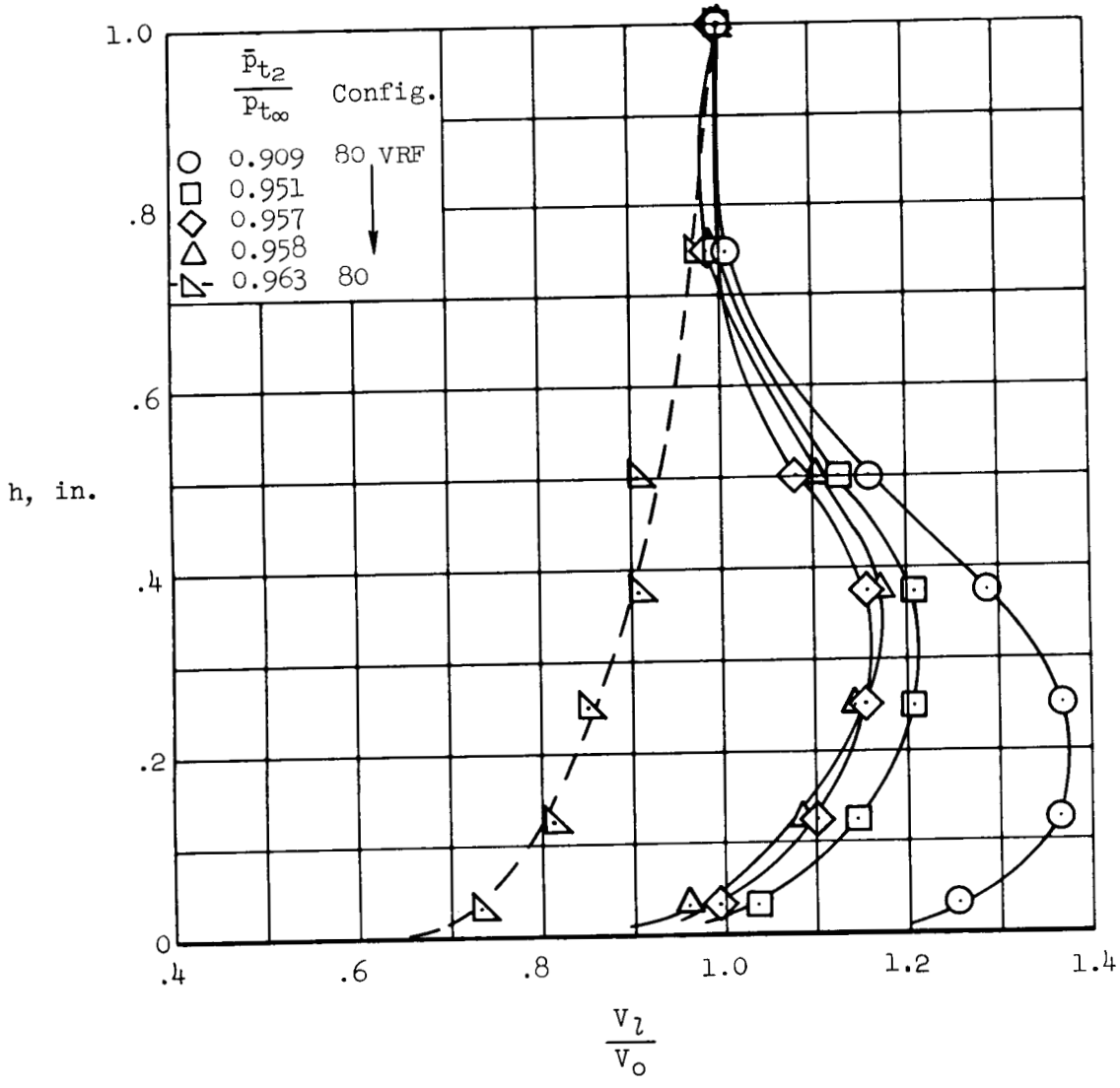

(c) $M_\infty = 2.00$

Figure 19.- Continued.

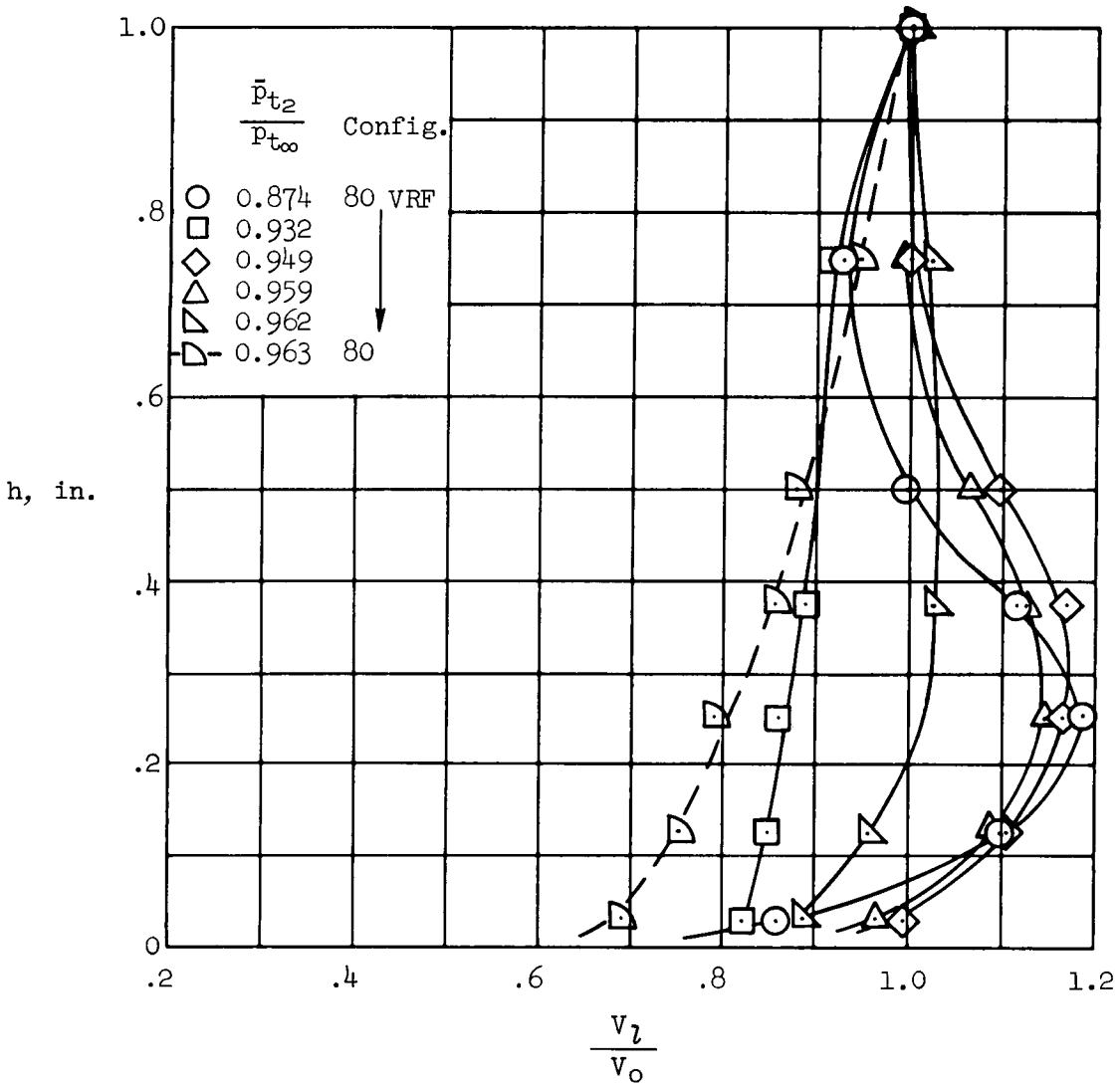

(d) $M_\infty = 1.55$

Figure 19.- Concluded.

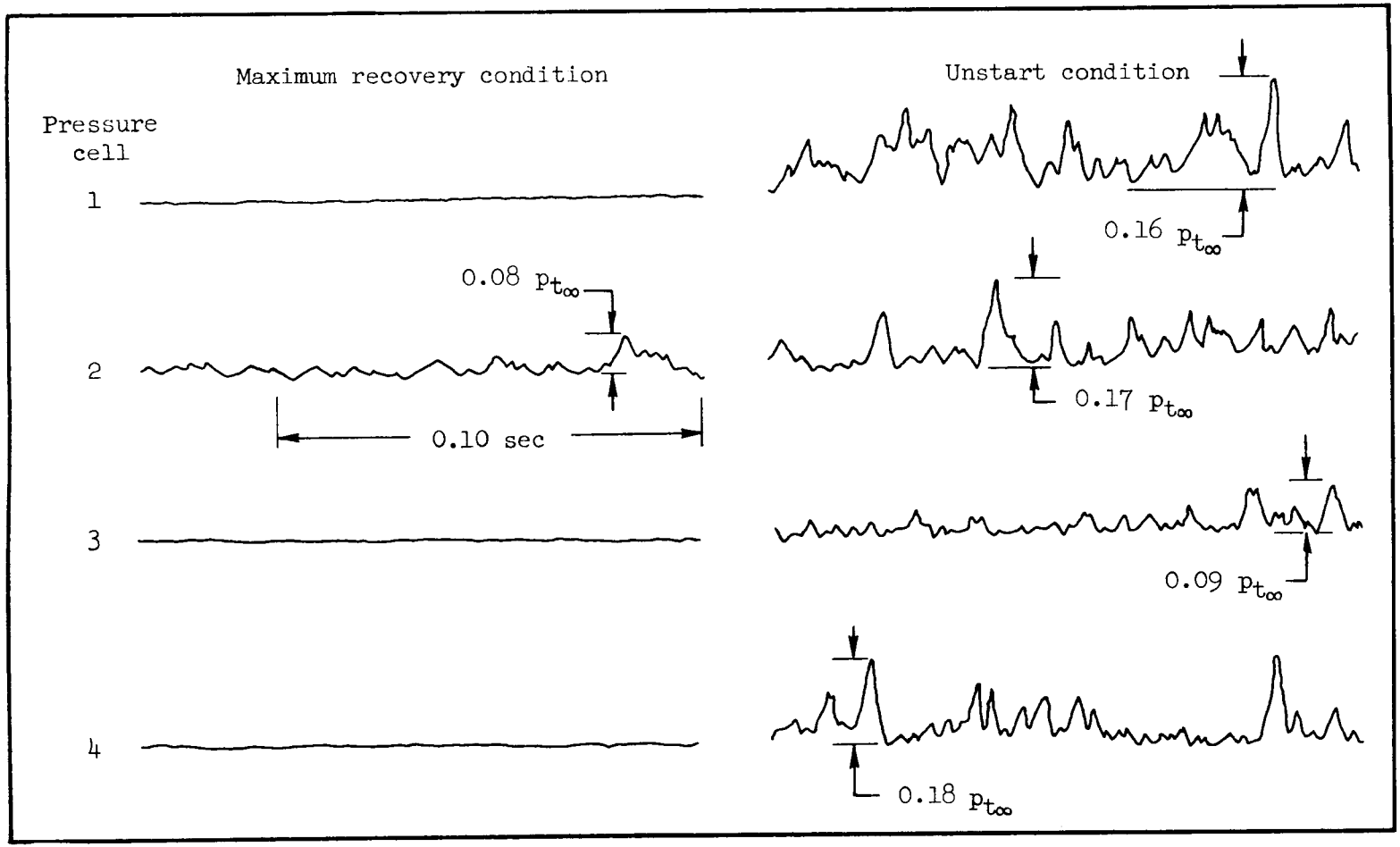

(a) $M_\infty = 3.00$

Figure 20.- Diffuser static-pressure unsteadiness characteristics.

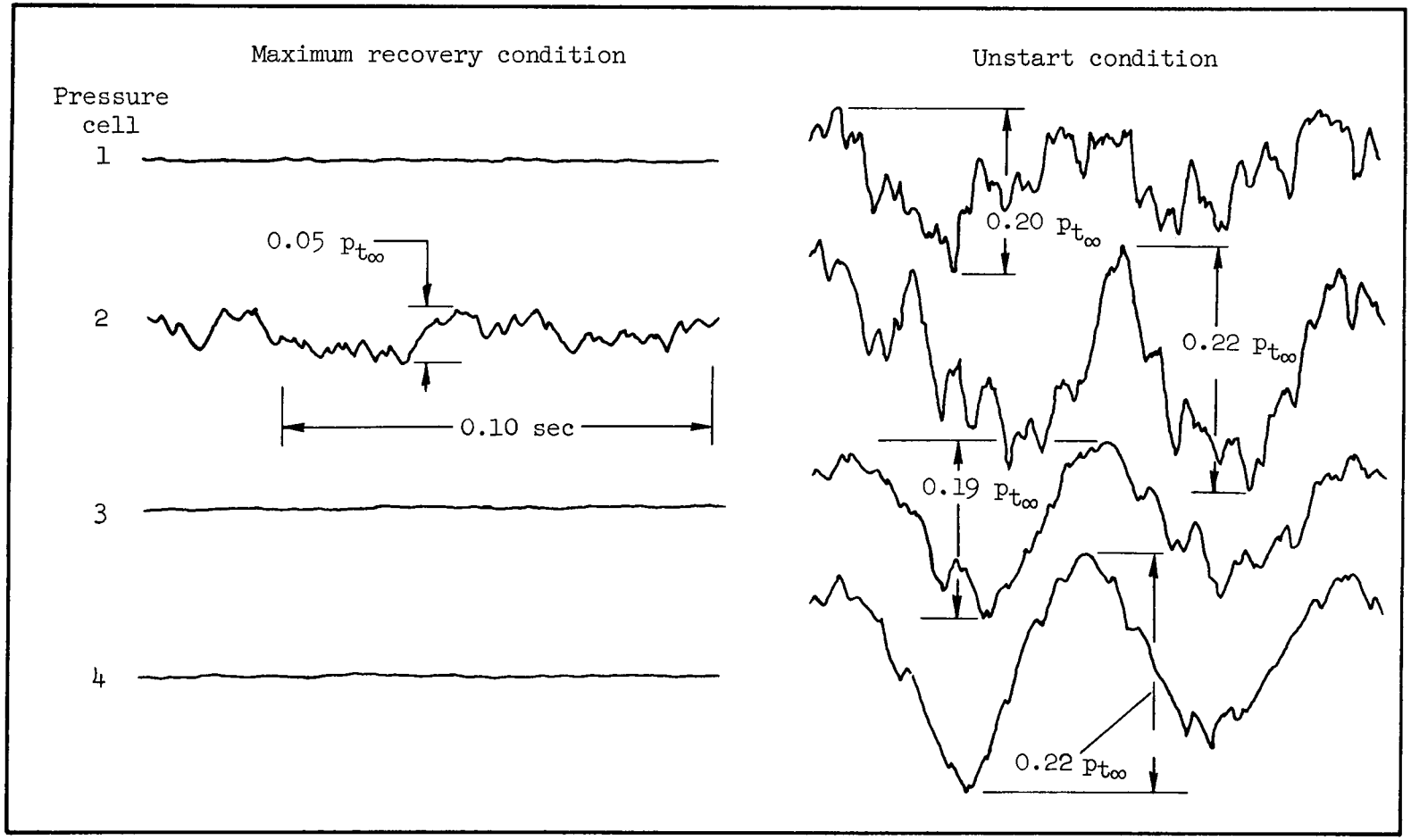

(b) $M_\infty = 2.50$

Figure 20.- Continued.

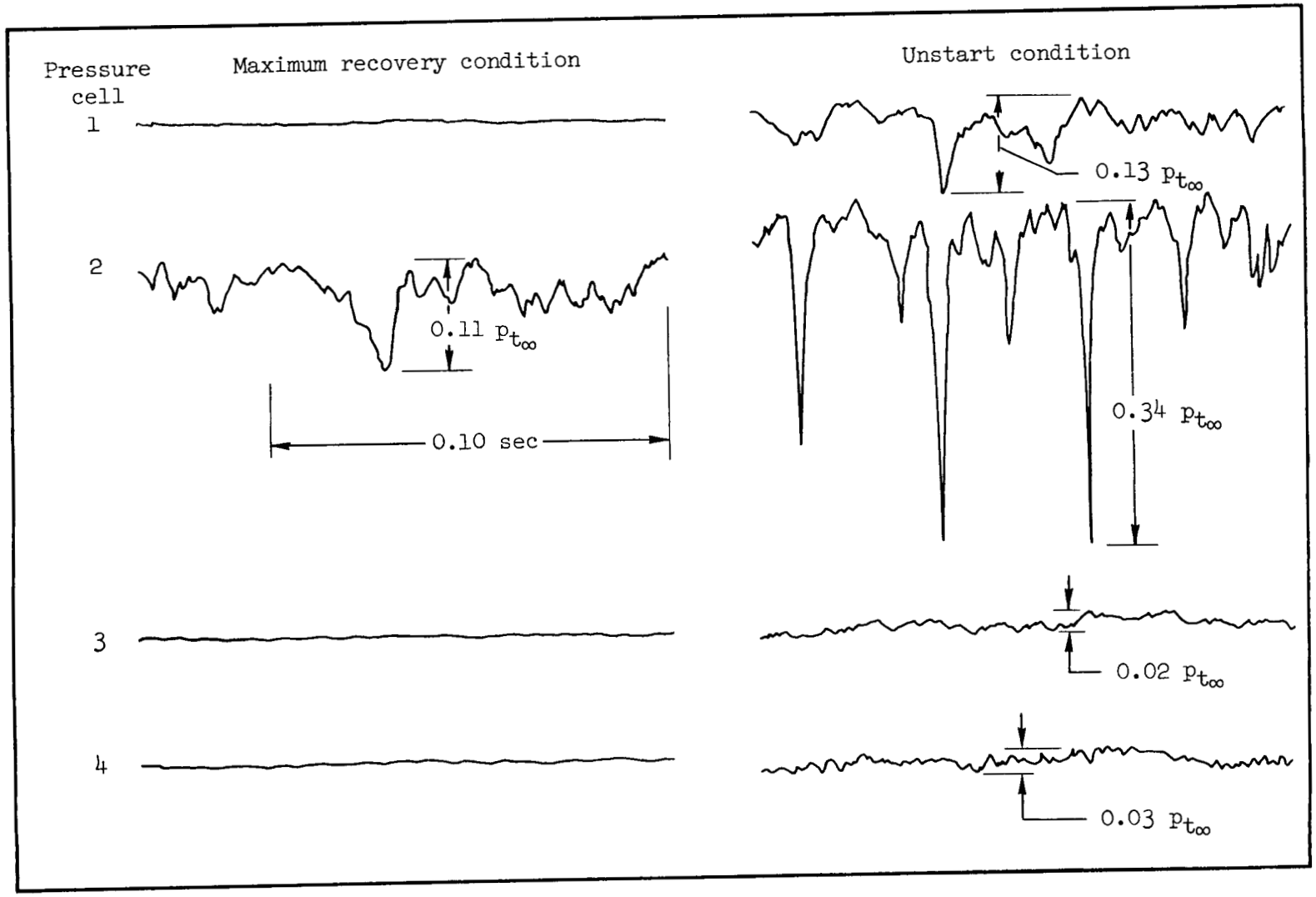

(c) $M_\infty = 2.00$

Figure 20.- Continued.

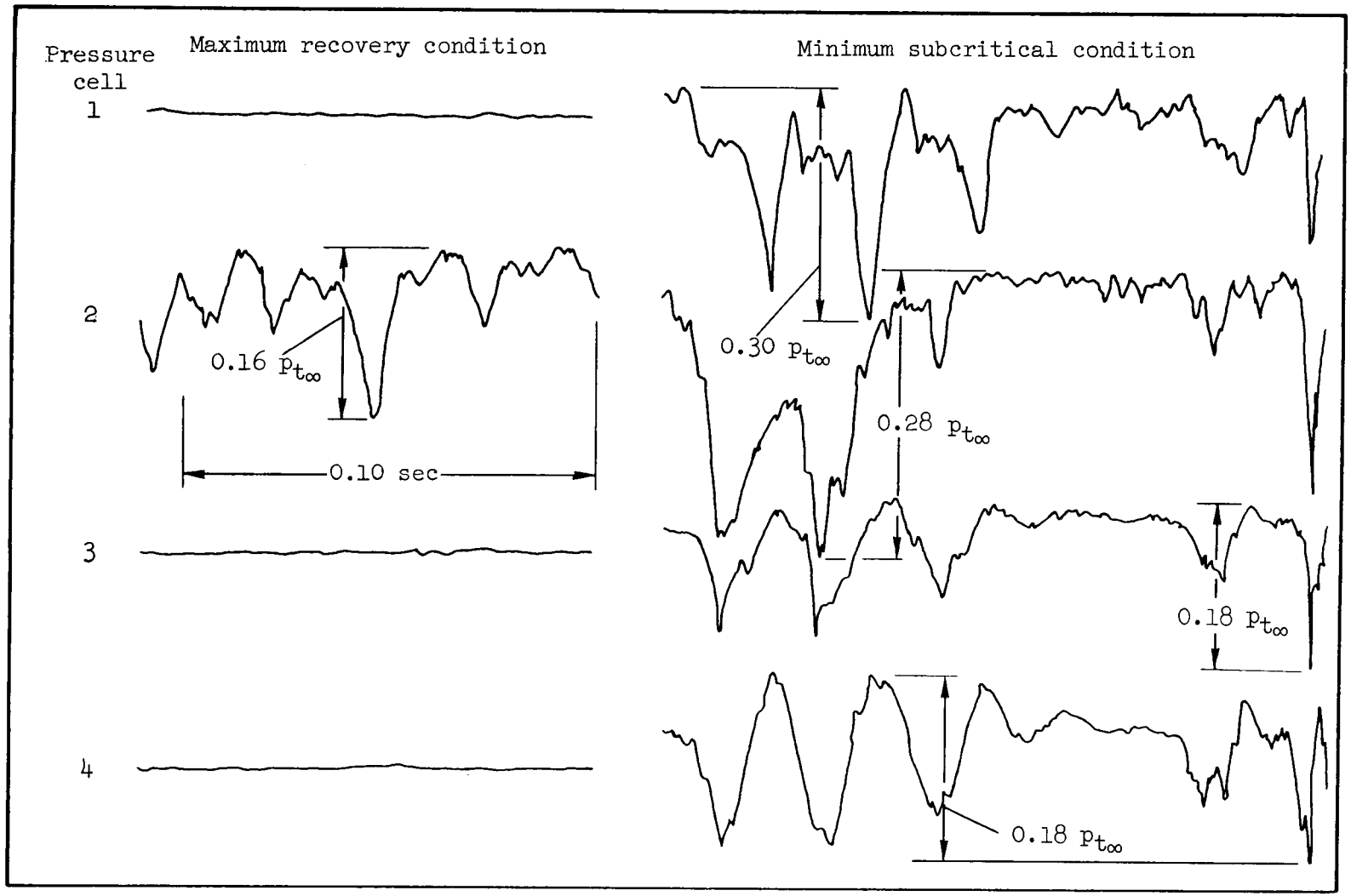

(d) $M_\infty = 1.55$

Figure 20.- Concluded.